ISTANBUL TECHNICAL UNIVERSITY ★ GRADUATE SCHOOL

PATH FOLLOWING OF AUTONOMOUS UNDERWATER VEHICLES IN THE PRESENCE OF UNKNOWN DISTURBANCES

M.Sc. THESIS

Muhammet AKAN

Department of Aeronautical and Astronautical Engineering

Aeronautical and Astronautical Engineering Programme

JUNE 2024

ISTANBUL TECHNICAL UNIVERSITY ★ GRADUATE SCHOOL

PATH FOLLOWING OF AUTONOMOUS UNDERWATER VEHICLES IN THE PRESENCE OF UNKNOWN DISTURBANCES

M.Sc. THESIS

Muhammet AKAN
(511211128)

Department of Aeronautical and Astronautical Engineering

Aeronautical and Astronautical Engineering Programme

Thesis Advisor: Prof. Dr. Cengiz HACIZADE

JUNE 2024

ISTANBUL TEKNİK ÜNİVERSİTESİ ★ LİSANSÜSTÜ EĞİTİM ENSTİTÜSÜ

OTONOM SUALTI ARAÇLARININ BİLİNMEYEN BOZUNTULARIN VARLIĞINDA YOL TAKİBİ

YÜKSEK LİSANS TEZİ

Muhammet AKAN
(511211128)

Uçak ve Uzay Mühendisliği Anabilim Dalı

Uçak ve Uzay Mühendisliği Programı

Tez Danışmanı: Prof. Dr. Cengiz HACIZADE

HAZİRAN 2024

Muhammet Akan, a M.Sc. student of İTU Graduate School student ID 511211128, successfully defended the thesis/dissertation entitled “Path Following of Autonomous Underwater Vehicles in the Presence of Unknown Disturbances”, which he prepared after fulfilling the requirements specified in the associated legislations, before the jury whose signatures are below.

Thesis Advisor :	**Prof. Dr. Cengiz HACIZADE** İstanbul Technical University	.....
Jury Members :	**Dr. Barış BAŞPINAR** Istanbul Technical University	.....
	Dr. Tuncay Yunus ERKEÇ National Defense University	.....

Date of Submission : 19 May 2024
Date of Defense : 25 June 2024

To my parents and fiancee,

FOREWORD

This thesis is the product of a comprehensive study that I prepared with intense effort and dedication in order to receive my Master's degree. The experiences I had and the knowledge I gained during this process were an important turning point in my career.

I would like to express my gratitude to my thesis advisor, Prof. Dr. Cengiz Hacızade, for his guidance, encouragement, and valuable suggestions. His wisdom and supportive attitude made this thesis more in-depth and comprehensive.

I would also like to express my endless gratitude to my beloved family and fiancee, who supported me every step of the way. Their patience, love, and faith were one of the most important factors that kept me alive during this difficult process.

I sincerely thank everyone who contributed to the completion of this thesis. Your valuable contributions enabled the successful completion of this study.

Finally, I hope that this thesis will contribute to the scientific community and the relevant field. I think this study will inspire future researchers.

June 2024

Muhammet AKAN
(Aeronautical Engineer)

TABLE OF CONTENTS

Page

ABBREVIATIONS

ALOS : Adaptive Line-Of-Sight
AUV : Autonomous Underwater Vehicle
AUVs : Autonomous Underwater Vehicles
DRL : Deep Reinforcement Learning
DVL : Doppler Velocity Log
EKF : Extended Kalman Filter
ELOS : Estimation of Line Of Sight
GPS : Global Positioning System
ILOS : Integral Line-Of-Sight
IMU : Inertial Measurement Unit
LMPC : Lyapunov-based Model Predictive Control
LOS : Line-Of-Sight
LTI : Linear Time Invariant
LQR : Linear Quadratic Regulator
MPC : Model Predictive Control
PID : Proportional Integral Derivative
RL : Reinforment Learning
RPM : Revolution Per Minute
STW : Speed Through Water
UKF : Unscented Kalman Filter
USBL : Ultra-Short Baseline

SYMBOLS

U	**:** Speed
$\mathbf{a_x, a_y, a_z}$	**:** Acceleration Components
x,y,z	**:** Position components
u,v,w	**:** Body Velocity Vector Components
p,q,r	**:** Angular Velocity Components
μ	**:** Mean
ϕ	**:** Roll Angle
θ	**:** Pitch Angle
Ψ	**:** Yaw Angle
σ	**:** Standard Deviation
$\boldsymbol{\sigma^2_{acc}}$	**:** Variance of Accelerometer
$\boldsymbol{\sigma^2_{gyro}}$	**:** Variance of Gyroscope

LIST OF TABLES

Page

LIST OF FIGURES

Page

PATH FOLLOWING OF AUTONOMOUS UNDERWATER VEHICLES IN THE PRESENCE OF UNKNOWN DISTURBANCES

SUMMARY

First of all, this study can be briefly explained as follows. It is about the path following of autonomous underwater vehicles (AUVs) when exposed to external environmental factors such as currents in predefined paths. In this study, algorithms were developed to solve the relevant problem based on the dynamic model of the Remus-100 autonomous underwater vehicle (AUV).

In this context, the performances of three guidance methods are compared to solve the problem, these guidance methods are line of sight (LOS) guidance, integrated line of sight(ILOS) guidance, and adaptive line of sight(ALOS) guidance. Additionally, a linear quadratic regulator (LQR) controller was designed to control the AUV. The states of the autonomous underwater vehicle, which is the input of the autopilot, were estimated using the Extended Kalman filter(EKF).

The reason for this study is that AUVs are being used a lot today and path following is critical in these vehicles. To briefly mention the usage areas of AUVs, these technologies are used in scientific research about oceanography, marine biology, mapping the seafloor, environmental monitoring about pollution levels, and geology research of the seafloor. In addition, AUVs may be used in military and defense for underwater surveillance and anti-submarine warfare. These vehicles are used in oil and gas exploration to inspect and map underwater pipelines and infrastructure. Additionally, they are operated in search and rescue operations to find missing ships and airplanes. Finally, they can be used in commercial fishing to help fishermen determine the best fishing locations and underwater archaeology to explore and map the underwater archaeological sites.

These usage areas bring with them an important problem that needs to be solved with high accuracy, and this is the path-following problem. These vehicles must follow predefined paths with high accuracy, even with limited position information and in situations where they are exposed to current disturbance. Otherwise, these vehicles cannot successfully perform the defined tasks. In this study, a solution to the 2-D path following problem is presented. The sub-topics focused on solving the problem are the design of the navigation, guidance, and autopilot algorithms of the AUV. Briefly, the navigation algorithm is the algorithm that calculates where and in what orientation the underwater vehicle is at the moment. The guidance algorithm calculates the heading angle that the underwater vehicle should apply to follow the path defined in 2-D. The autopilot algorithm ensures that the underwater vehicle is kept in the desired orientation. As a result, these algorithms must work properly simultaneously for the AUV to follow a defined path.

When first focusing on the navigation algorithm, its output is also the reference input of the autopilots of underwater systems operating in real-time. In this context, these inputs need to be estimated and measured accurately. In addition, if a state that is not directly measured is to be used as an input to the autopilot, this state needs to be estimated. In addition, for the autopilot to produce proper outputs, the noise level of

noisy measurement data produced from sensor models must be reduced, and this can be made possible with EKF.
In addition, this AUV is exposed to the effects of underwater currents during its operations. This disturbance can create major problems in docking missions where location accuracy is important and in long-term missions such as military applications or mapping. Therefore, these disturbance components need to be estimated. In this context, using the EKF, the AUV's position components, velocity components, acceleration components, Euler angles, angular rates, and sea current components will be estimated. The sensors to be used when making these predictions are an ultra short base line (USBL) acoustic positioning system, inertial measurement unit (IMU), depth sensor, compass, and Doppler velocity log (DVL). The reason for using EKF is that it can be easily applied to nonlinear systems, with its prediction accuracy, adaptability, and simplicity.
In this study, autopilots were designed using the LQR technique. The LQR method offers a robust framework for control design, optimizing control inputs to minimize a specified cost function while considering system dynamics and constraints. This study applies LQR to the nonlinear dynamics of AUV by first linearizing the model using numerical techniques. This allows for the formulation of the control problem in a linear framework, where LQR can effectively compute feedback gains to steer the system towards desired states.
The primary advantage of utilizing LQR lies in its ability to provide stable and efficient control across a range of operating conditions. By optimizing a quadratic performance index, LQR ensures that the AUV achieves the desired performance while adhering to system constraints. Furthermore, the straightforward implementation process of LQR simplifies the design and facilitates real-time deployment on AUV platforms. This enables the development of robust autopilot systems capable of navigating complex underwater environments. As a result, when the LQR controller was tested under various conditions, it was seen that it worked with high performance and low control effort even in disturbed environments.
Finally, it is briefly mentioned that the guidance methods used in the path following strategy, LOS, ILOS, and ALOS guidance methods were used in this study. These guidance algorithms take as input the waypoints of the path they need to follow and the currently calculated position of the AUV. As output, they calculate the heading angle the AUV should apply to follow this path. The calculated heading command gives satisfactory results in path following in 2-D for autonomous underwater vehicles. In these methods, the location information given as input is the location information that is the output of EKF. In addition, the vehicle's states used as reference in autopilots are also components calculated by EKF. The dynamic model output of the vehicle was not used as input in the autopilot and guidance algorithms, these inputs were the outputs of the EKF. If dynamic model outputs were used, reliable results could not be obtained in testing the usability of these algorithms in real life. Therefore, the outputs of the dynamic model were used as ground truth and the actual states of the vehicle were converted into sensor outputs using sensor models. States that were not directly measured by sensors were estimated with EKF. With this approach, an attempt was made to simulate a real AUV operation.
During the testing phase, 4 different paths were defined and tested. The first of these paths is a straight path, the second is a circular path, and the third is a path where both a straight route and turning maneuvers are made. The last path is sinusoidal. While testing these paths, current disturbance was added to the environment, and in this way, it was aimed to test situations where the vehicle was exposed to current disturbance.

In this context, tests were carried out with 3 current speed components and 4 current direction components. These tests compared the performance of 3 different guidance algorithms in different current components and path definitions. The cross-track error component, which calculates the distance from the path, was used as the comparison parameter. Finally, it was concluded that some guidance laws are more advantageous in certain situations. Briefly speaking, ILOS guidance law shows superior performance in circular and sinusoidal paths, which shows that ILOS guidance gives better results in paths containing curvature. It has been observed that LOS guidance giving good results on straight and semi-rectangular paths, which shows that LOS guidance gives better results on flat paths compared to other methods. In this case, it can be concluded that since the defined paths are predetermined paths, if there are straight lines in the planned path, LOS guidance can be used during this process, and ILOS guidance can be used actively in the parts of the path that contain curvatures, that is, in places where there are turns and maneuvers. This ultimately enables maximum path-following performance to be achieved in all designed paths. Since one guidance law performs better than the other according to the path features, automatic guidance law switching can be performed in AUV tasks by establishing a simple switch-case logic and achieving minimum cross-track error. One of the most important results of this study can be explained as follows: Depending on the characteristics of the defined path, the guidance law may change during the mission because the currently used guidance laws calculate the yaw angle command as a result of instantaneous calculations, that is, they do not contain any retrospective terms. Therefore, transitions between these algorithms do not create any discontinuity. Finally, all of the algorithms developed within the scope of this study have been developed to be used in real underwater vehicles, so I believe that the algorithms to be developed for Remus-100 in the future can be used as a reference source.

OTONOM SUALTI ARAÇLARININ BİLİNMEYEN BOZUNTULARIN VARLIĞINDA YOL TAKİBİ

ÖZET

İlk olarak, bu tezin çalışma konusu otonom su altı araçlarının, akıntılar gibi dış çevre faktörlerine maruz kaldığında, önceden tanımlanmış yolları takip edebilmesi problemine çözüm sunulması ile ilgilidir. Bu çalışmada, Woods Hole Oşinografi Enstitüsü tarafından geliştirilen Remus-100 otonom su altı aracının dinamik modeli referans alınmıştır. İlgili problemin çözümüne yönelik algoritmalar bu dinamik model kullanılarak geliştirilmiştir.

Bu kapsamda, bu problemin çözümüne yönelik üç farklı güdüm yöntemi uygulanmış ve test edilmiştir. Çalışmanın sonucunda da bu üç farklı güdüm yönteminin performansları karşılaştırılmıştır. Bu güdüm yöntemleri görüş hattı güdümü, integral görüş hattı güdümü ve adaptif görüş hattı güdümü algoritmalarıdır. Bu otonom su altı aracının otopilotu için LQR kontrolcü tasarlanmıştır. Otopilotun girdisi olan su altı aracının durumları, Genişletilmiş Kalman filtresi kullanılarak kestirilmiştir.

Bu çalışmanın nedeni otonom su altı araçlarının günümüzde çok fazla kullanılmaya başlanmasıdır ve bu araçların kullanımında yol takibinin kritik olmasıdır. Bu araçların kullanım alanlarına kısaca değinmek gerekirse bu araçlar, oşinografi, deniz biyolojisi, deniz tabanının haritalanması, kirlilik seviyelerinin çevresel izlenmesi ve deniz tabanının jeoloji araştırmaları ile ilgili bilimsel araştırmalarda kullanılmaktadır. Ek olarak, bu araçlar askeri alanda ve savunmada su altı gözetleme ve denizaltı karşıtı savaş için kullanılabilmektedir. Ayrıca bu araçlar, petrol ve doğalgaz aramalarında, su altı boru hatlarını ve altyapısını incelemek ve haritalamak için kullanılmaktadır. Ek olarak kayıp gemi ve uçakların bulunmasına yönelik arama kurtarma operasyonlarında da görev almaktadırlar. Son olarak, balıkçıların en iyi balık avlama yerlerini belirlemelerine ve su altı arkeolojik alanlarını keşfetmeleri ve haritalandırmaları için su altı arkeolojisine yardımcı olmak amacıyla kullanılabilmektedirler.

Bu kullanım alanları yüksek doğrulukla çözülmesi gereken önemli bir problemi de beraberinde getirmektedir ve bu problem yol takibi problemidir. Bu araçların, sınırlı konum bilgisine sahip oldukları durumlarda ve su akıntısına maruz kaldıkları durumlarda bile önceden tanımlanmış yolları yüksek doğrulukla takip etmeleri gerekmektedir. Aksi takdirde bu araçlar tanımlanan görevleri başarıyla yerine getiremezler. Bu çalışmada 2 boyutta yani x-y düzleminde tanımlanan bir yolun takibi problemine bir çözüm sunulmuştur.

Bu çalışmada bu problemin çözülmesi için odaklanılan alt konular ise, otonom su altı aracının navigasyon, güdüm ve otopilot algoritmalarının tasarımıdır. Bu çalışmada ortaya konulan navigasyon algoritmasından kısaca bahsedilirse, su altı aracının o an nerede ve hangi oryantasyonda olduğunu hesaplayan algoritmadır. Güdüm algoritması ise, su altı aracının 2 boyutta tanımlanan yolu takip edebilmesi için uygulaması gereken rota açısını hesaplar. Otopilot algoritması ise, su altı aracının istenilen oryantasyonda tutulmasını sağlar. Sonuç olarak su altı aracının belirli bir yolu takip edebilmesi için bu algoritmaların eş zamanlı olarak düzgün çalışması gerekmektedir.

Bu çalışmada navigasyon algoritmasının kapsamına bakıldığında, genişletilmiş Kalman filtresi kullanılarak sualtı aracının bazı durum bileşenlerinin kestirim yolu ile elde edilmesi olarak tanımlanabilir. Navigasyon algoritması çıktısı aynı zamanda otopilotun referans girdisidir. Bu bağlamda bu girdilerin doğru bir şekilde otopilota sağlanması gerekmektedir. Ayrıca doğrudan ölçülmeyen bir durum otopilota girdi olarak sağlanması durumunda, bu durum bileşeninin kestirilmesi gerekir. Ek olarak, otopilotun kararsızlığa neden olmayacak çıktılar üretebilmesi için sensör modellerinden üretilen gürültülü ölçüm verilerinin gürültü düzeyinin azaltılması gerekmektedir ve bu da genişletilmiş Kalman filtresi ile mümkün kılınabilmektedir.
Ayrıca bu araç, operasyonu sırasında su altı akıntılarının etkilerine de maruz kalmaktadır. Bu bozuntu, konum doğruluğunun önemli olduğu görevlerde büyük sorunlar yaratabilmektedir. Bu nedenle bu akıntı bozuntusunun bileşenlerinin kestiriminin yapılması gerekmektedir. Bu kapsamda genişletilmiş Kalman filtresi kullanılarak bu otonom sualtı aracının konum bileşenleri, hız bileşenleri, ivme bileşenleri, Euler açıları, açısal hızları ve maruz kaldığı deniz akıntısının bileşenleri kestirilmiştir. Bu kestirimleri yaparken kullanılan sensörler, ultra kısa baz hattı akustik konumlandırma sistemi, atalet ölçüm birimi, derinlik sensörü, pusula ve Doppler hız ölçeridir. Kestirim sonuçları değerlendirildiğinde, oldukça yüksek doğrulukta sonuçlar elde edildiği görülmüştür. Genişletilmiş Kalman filtresi kullanılmasının nedeni tahmin doğruluğu, uyarlanabilirliği ve basitliği ile doğrusal olmayan sistemlere kolaylıkla uygulanabilmesidir.
Bu çalışmada otopilotlar Lineer Kuadratik Regülatör tekniği kullanılarak tasarlanmıştır. LQR yöntemi, sistem dinamiklerini ve kısıtlamalarını dikkate alırken, aynı zamanda belirli bir maliyet fonksiyonu tanımlanarak maliyeti en aza indirmek için kontrol girdilerini optimize etmeye olanak sağlar. Bu tasarım yaklaşımında öncelikle kontrol edilmek istenen sistemin lineer modeline sahip olunması gereklidir. Fakat bu çalışmada kurulan model 6 serbestlik derecesine sahip ve tamamıyla lineer olmayan bir modelden oluşmaktadır. Bu yüzden önce numerik doğrusallaştırma tekniği kullanılarak model doğrusallaştırıldı. Bu sayede problem, tipik LQR problemine dönüşmüş olur ve sistemin durum uzay gösterimleri elde edilmiş olur. Sonrasında durum ve girdilerin ağırlık matrisleri tasarım parametreleri olarak belirlendi ve kontrolcünün tasarım süreci tamamlanmıştır.
LQR kullanmanın temel avantajı, çeşitli çalışma koşullarında stabil ve verimli kontrol sağlama yeteneğinde yatmaktadır. Bu çalışmada, LQR kontrolcü ikinci dereceden bir performans endeksini optimize ederek AUV'nin sistem kısıtlamalarına bağlı kalarak istenen performansı elde etmesini sağlar. Ayrıca bu kontrol metodolojisinin basit uygulama süreci, tasarımı basitleştirir ve gerçek zamanlı AUV platformlarında tasarımı kolaylaştırır. Ayrıca otopilot döngüsü kompleks hesaplamalar içermediği için hesaplama zamanı çok düşüktür. Bu durum, karmaşık su altı ortamlarında seyir yapılmasına olanak sağlayan gürbüz otopilot sistemlerinin geliştirilmesine olanak sağlar. Sonuç olarak bu tez çalışmasında tasarlanan LQR kontrolcü, çeşitli koşullar altında test edildiğinde, bozulmuş ortamlarda dahi yüksek performansla ve düşük kontrol eforuyla çalıştığı görülmüştür.
Son olarak bu çalışmada yolu takip etme stratejisinde kullanılan güdüm yöntemleri olan görüş hattı güdümü, integral görüş hattı güdümü ve adaptif görüş hattı güdümü algoritmaları kullanıldığına kısaca değinilmişti. Bu güdüm algoritmaları, takip etmeleri gereken yolun ara noktalarını ve su altı aracının o anda hesaplanan konumunu girdi olarak alır. Çıktı olarak su altı aracının bu yolu takip etmesi için uygulaması gereken rota açısını hesaplarlar.

Hesaplanan rota komutu, bu otonom su altı aracı için 2 boyutlu yol takibinde yapılan testler sonucunda tatmin edici sonuçlar vermektedir. Bu yöntemlerde girdi olarak verilen konum bilgisi genişletilmiş Kalman filtresinin çıktısı olan konum bilgisidir. Ayrıca aracın otopilotlarda referans olarak kullanılan durumlarda genişletilmiş Kalman filtresi tarafından hesaplanan bileşenlerdir. Burada önemli bir noktaya değinmek gerekir, aracın dinamik model çıktıları otopilot ve güdüm algoritmalarında girdi olarak kullanılmamıştır, bu girdiler için genişletilmiş Kalman filtresi kullanılmıştır. Dinamik model çıktılarının kullanılması halinde bu algoritmaların gerçek hayatta kullanılabilirliğinin test edilmesinde güvenilir sonuçlar elde edilemeyecektir.

Bu nedenle dinamik modelin çıktıları kesin referans olarak kullanıldı ve bu referans hata hesaplamalarında kullanıldı. Ayrıca sensör modelleri geliştirildi ve aracın gerçek durumları yani kesin referans olarak kullanılan durumlar, sensör modellerine girdi olarak girip sensör çıktılarına dönüştürülmüştür. Sensörler tarafından doğrudan ölçülmeyen durumlar ise genişletilmiş Kalman filtresi ile kestirilmiştir. Bu yaklaşımla gerçek bir otonom sualtı aracı operasyonu simüle edilmeye çalışılmıştır. Bu geliştirilen algoritmaların test aşamasında ise 4 farklı yol tanımlandı ve test edildi. Bu yollardan ilki dairesel bir yol, ikincisi düz bir yol, üçüncüsü ise hem düz bir rota hem de dönüş manevralarının yapıldığı bir yoldur. Son yol ise sinüzoidal bir yol olarak tanımlanmıştır.

Geliştirilen yol takibi algoritması, bu yollarda test edilirken ortama su akımı bozuntusu eklenmiş ve bu şekilde aracın akım bozuntusuna maruz kaldığı durumların test edilmesi amaçlanmıştır. Bu kapsamda 3 adet akım hız bileşeni ve 4 adet akım yönü bileşeni ile testler gerçekleştirilmiştir. Bu testler ile farklı akım bileşenleri ve yol tanımlarında 3 farklı güdüm algoritmasının performanslarının karşılaştırılması amaçlandı. Karşılaştırma parametresi olarak yola olan mesafeyi hesaplayan geçiş izi hatası bileşeni kullanılmıştır. Son olarak bazı güdüm yasalarının belirli durumlarda daha avantajlı olduğu sonucuna varılmıştır. Kısaca söylemek gerekirse, integral görüş hattı güdümü yasası dairesel ve sinüzoidal yollarda üstün performans göstermektedir, bu da bu metodun eğrilik içeren yollarda daha iyi sonuçlar verdiğini göstermektedir. Görüş hattı güdümü yasasının ise düz ve yarı dikdörtgen yollarda iyi sonuçlar verdiği gözlemlenmiştir, bu da bu metodun düz yollarda diğer yöntemlere göre daha iyi sonuçlar verdiğini göstermektedir. Bu durumda tanımlanan yollar önceden belirlenmiş yollar olduğundan, planlanan yolda düz çizgiler varsa bu süreçte görüş hattı güdümü yasasından yararlanılabileceği gibi, yolun kalan kısımlarında da integral görüş hattı güdümü aktif olarak yararlanılabileceği sonucuna varılabilir. Eğrilikler, yani dönüşlerin ve manevraların olduğu yerlerde bu yasanın kullanılması daha uygun olabilir. Bu yaklaşım ile tasarlanan tüm yollarda maksimum yol izleme performansının elde edilmesini sağlanır. Yol özelliklerine göre bir güdüm yasası diğerinden daha iyi performans gösterdiğinden, basit bir anahtarlama durumu mantığı kurularak ve minimum geçiş izi hatası elde edilerek AUV görevlerinde otomatik güdüm yasası geçişi gerçekleştirilebilir. Bu çalışmanın en önemli sonuçlarından biri şu şekilde açıklanabilir, tanımlanan yolun özelliklerine bağlı olarak, mevcut kullanılan güdüm yasaları sapma açısı komutunu anlık hesaplamalar sonucunda hesapladığından, görev sırasında güdüm yasası değişebilir, yani geriye dönük herhangi bir terim içermezler. Dolayısıyla bu algoritmalar arasındaki geçişler herhangi bir süreksizlik yaratmamaktadır. Son olarak bu çalışma kapsamında geliştirilen algoritmaların tamamı gerçek su altı araçlarında kullanılmak üzere geliştirilmiştir.

1. INTRODUCTION

Autonomous Underwater Vehicles (AUVs) have emerged as cutting-edge technologies revolutionizing underwater exploration and research. These unmanned vehicles, equipped with advanced sensors and autonomous navigation systems, are reshaping our understanding of the underwater world. Their popularity stems from several key factors contributing to their widespread adoption and recognition in modern times.

Nowadays, the use of these vehicles is common, to give a few examples, they can be listed as follows. These vehicles are used in scientific research about oceanography, marine biology, mapping the seafloor, environmental monitoring about pollution levels, and geology research of the seafloor. In addition, AUVs may be used in military, defense for underwater surveillance and anti-submarine warfare. These vehicles are used in oil and gas exploration to inspect and map underwater pipelines and infrastructure. Additionally, they are operated in search and rescue operations to find missing ships and airplanes. Finally, they can be used in commercial fishing to help fishermen determine the best fishing locations and underwater archaeology to explore and map the underwater archaeological sites[1].

In AUVs, one of the fundamental challenges encountered across various applications is the concept of path following. Path following refers to the ability of an AUV to navigate and track a predefined path or trajectory accurately and robustly, even in the presence of external disturbances such as underwater currents, varying terrain, or environmental uncertainties.

The importance of path following cannot be overstated, as it directly influences AUV operations' efficiency, reliability, and effectiveness across a wide range of domains. Whether conducting scientific research missions, environmental monitoring surveys, industrial inspections, or security and defense operations, AUVs must possess robust path following capabilities to fulfill their intended objectives and navigate safely in dynamic underwater environments.

The motivation behind focusing on addressing the path following problem lies in the critical role it plays in maximizing the utility and performance of AUVs. Accurate path following enables AUVs to collect precise data, execute complex tasks, and achieve mission objectives with greater precision and efficiency. Moreover, robust path following capabilities contribute to the safety of AUV operations, minimizing the risk of collisions, deviations from desired trajectories, and potential mission failures.

In this study, the primary objective is to develop and evaluate novel path following algorithms and control strategies specifically tailored for AUVs operating in challenging underwater conditions. By enhancing the path following capabilities of AUVs, this research aims to overcome the limitations posed by external disturbances and environmental uncertainties, ultimately enabling AUVs to navigate autonomously and effectively in real-world scenarios.

In summary, path following represents a cornerstone of AUV technology, underscoring its significance in enabling autonomous navigation and enhancing its overall performance and utility in various underwater applications. By addressing the path following problem, this study seeks to advance the capabilities of AUVs and pave the way for their expanded use and impact in underwater exploration, research, and industrial operations.

1.1 Problem Description

The focus of this study revolves around the challenge of achieving reliable path following by autonomous underwater vehicles (AUVs) in environments affected by disturbances such as underwater currents. Path following is a critical capability for AUVs as it enables them to navigate predefined trajectories accurately, ensuring successful completion of missions and tasks in dynamic underwater environments. However, the presence of disturbances like underwater currents poses significant challenges to the path following capabilities of AUVs, leading to deviations from desired trajectories and potentially hindering mission success.

To address this challenge, the study investigates the implementation and performance comparison of three distinct guidance methods: Line-Of-Sight (LOS), Integral Line-Of-Sight (ILOS), and Adaptive Line-Of-Sight (ALOS). These guidance methods are designed to calculate the heading angle required to track predefined paths in the x-y plane based on waypoint inputs. By comparing the performance of these guidance

methods under various test scenarios, the study aims to identify the most effective approach for achieving robust path following by AUVs in the presence of disturbances.
The methodology employed in this study involves several key steps. Initially, a dynamic model of the REMUS-100 AUV is utilized, supplemented with sensor models including an Inertial Measurement Unit (IMU), Doppler Velocity Log (DVL), compass, and Ultra-Short Baseline (USBL) sensors. The outputs of these sensor models are integrated using an Extended Kalman Filter (EKF) to estimate the states of the underwater vehicle, which serve as inputs to the designed autopilot. The autopilot is designed using Linear Quadratic Regulator (LQR) control technique, linearizing the nonlinear REMUS-100 model through numerical linearization.
Subsequently, the designed guidance algorithms are implemented to compute the required heading angles for path following in the x-y plane. Four different paths are defined for testing purposes, and the performance of the guidance methods is evaluated based on their ability to track these paths accurately in the presence of disturbances.
In summary, the overarching goal of this study is to address the challenge of achieving reliable path following by AUVs in environments affected by disturbances, such as underwater currents. By comparing the performance of different guidance methods, the study aims to identify the most suitable approach for enhancing the path following capabilities of AUVs, thereby contributing to advancements in underwater robotics and autonomous navigation technologies.

1.2 Contribution of This Study

The findings of this study are anticipated to make significant contributions to the field of AUV path following in environments affected by disturbances. This research aims to enhance the understanding of effective strategies for autonomous path following in dynamic underwater environments by investigating and comparing different guidance methods for path following under challenging conditions.
Firstly, the study has the potential to advance the development of robust guidance algorithms tailored for AUVs operating in real-world scenarios. By evaluating and comparing the performance of distinct guidance methods, researchers and practitioners can gain insights into the strengths and limitations of each approach, facilitating the selection and implementation of the most effective strategy for specific mission requirements.

Secondly, the study may contribute to the improvement of AUV capabilities in various applications, including scientific research, environmental monitoring, industrial inspections, and security operations. By enhancing the path following capabilities of AUVs, this research has the potential to enable more accurate and efficient data collection, mapping, and surveying in underwater environments, leading to advancements in our understanding of marine ecosystems, geological features, and underwater infrastructure.

Furthermore, the findings of this study could have implications for the development of autonomous navigation technologies beyond the field of underwater robotics. The insights gained from evaluating different guidance methods and control strategies may inform the design and optimization of autonomous systems operating in other dynamic and uncertain environments, such as aerial drones, terrestrial robots, and autonomous vehicles. In summary, the outcomes of this study are expected to contribute to the advancement of autonomous path following technologies, enhance the capabilities of AUVs in underwater exploration and research, and potentially inspire innovations in autonomous systems across various domains.

1.3 Literature Review

The literature review chapter examines current research on autonomous underwater vehicle (AUV) navigation and control, with a focus on path following and stabilization in dynamic underwater environments. It aims to summarize existing methodologies and advancements. Preliminarily, if the emphasis is on resolving the issue of path following a pre-established trajectory for underwater vehicles and ships, the subsequent investigations have been conducted thus far.

Firstly, it will be examined how this problem is addressed in the literature. A study focuses on path-following control strategies for asymmetry underactuated unmanned surface vehicles under external disturbances, it proposes an adaptive sliding-mode control system which is incorporating a modified integral line-of-sight guidance law and adaptive feedback linearizing controllers combined with sliding-mode techniques [2]. A separate study focuses on the issue of horizontal trajectory tracking for underactuated AUVs in the presence of parameter perturbation. The study proposes a trajectory tracking controller that consists of a kinematic controller designed using the backstepping method and a dynamic controller that utilizes global integral sliding

mode control to stabilize velocity errors. This approach guarantees the stability of the entire system [3]. Another study presents a solution for following a curved path in the presence of constant unknown ocean current disturbances, it employs a nonsingular path variable update law and a guidance law designed to reject these disturbances using an ocean current observer, this approach is resulting in globally asymptotically stable and locally exponentially stable path following errors [4]. Another work focuses on the problem of enabling unmanned marine vessels to autonomously follow a path, even when faced with unexpected ocean currents. It presents an approach that builds upon prior findings on the path following by incorporating a virtual Serret-Frenet reference frame that is based on the intended path. The suggested closed-loop system, comprising an ocean current observer, a guidance law, a controller, and an update law for the Serret-Frenet frame, has been proven to be uniformly globally asymptotically stable. The theoretical conclusions have been confirmed through simulation results [5]. Another study presents a PID controller that is designed to accurately track waypoints of hovering autonomous underwater vehicles. The controller is specifically tailored to follow arbitrary waypoints that are constructed as surveillance channels for offshore plant building. The controller consists of vertical and horizontal plane controllers. Simulation results confirm the controller's efficacy in accurately following all waypoints within a 1-meter error margin [6]. A separate study introduces a nonlinear adaptive controller designed to dynamically position and track waypoints for underactuated AUVs under environmental disturbances and uncertain parameter modeling. Initially developed at the kinematic level with assumed knowledge of ocean current perturbation, the controller utilizes an exponential observer for current estimation and incorporates integrator backstepping and Lyapunov-based techniques to handle modeling uncertainties in dynamic scenarios [7]. Another study proposes a robust control method for dynamically positioning and tracking waypoints of underactuated AUVs. The design of the controllers utilizes sliding mode control techniques to enhance their robustness [8]. In addition, another study introduces a novel method, deep interactive reinforcement learning, which combines deep reinforcement learning(RL) and interactive RL to enhance the AUV path following. Additionally, a method is proposed to learn from both human and environmental rewards simultaneously. Simulation results show that the approach achieves faster convergence than traditional deep Q-network learning with only environmental rewards. Moreover, it matches or surpasses the performance of deep interactive RL,

demonstrating adaptability to real-world environments [9]. In another study, it seeks to address the problem of trajectory tracking control for Autonomous Underwater Vehicles (AUVs) by enhancing deep reinforcement learning (DRL). The DRL methodology employs a pair of neural networks, one network is responsible for selecting actions, while the other network assesses the accuracy of these actions using deep deterministic policy gradient. These networks, which consist of numerous layers that are fully coupled, surpass typical PID control in accurately achieving trajectory tracking for AUVs that navigate intricate bends [10]. Additionally, another study introduces using nonlinear iterative sliding mode incremental feedback and the Serret-Frenet coordinate system. This approach effectively reduces overshoot and achieves precise horizontal path tracking for AUVs [11]. A sliding mode control law is developed and tested to guide underactuated autonomous surface vessels along trajectories. This control law utilizes first-order sliding surfaces for surge tracking errors and second-order ones for lateral motion tracking errors, which is ensuring precise position tracking while constraining rotational motion [12]. Another study introduces using a second-order sliding-mode controller to stabilize AUVs in the face of modeling errors and environmental perturbations for path-following missions. This control architecture compensates for uncertainties in the vehicle's hydrodynamic modeling parameters well [13]. Another work presents a strong nonlinear controller for AUVs, guaranteeing that the vehicles will eventually reach a predetermined path at a consistent speed. Originally designed as a kinematic controller, it has been enhanced to incorporate vehicle dynamics through the application of backstepping and Lyapunov algorithms. The hybrid adaptation technique ensures resilience to parameter ambiguity [14]. Another research introduces an optimization-based method for dynamical positioning of underwater vehicles in real-time. The system utilizes a hierarchical approach that involves two loops: a kinematic loop that uses nonlinear model predictive control to generate the required velocity, and a dynamic loop that use neural network model reference adaptive control to assure accurate velocity tracking even in the presence of uncertainties [15]. A separate study suggests a control approach for accurately following a desired trajectory and course with underactuated underwater vehicles. A control approach utilizing feedback linearization is devised. The method effectively addresses external disruptions such as ocean currents and is verified using Lyapunov analysis, showcasing global exponential stability [16].

In this study, the problem of path following was approached by developing an estimation algorithm to accurately determine the states of the AUV. Subsequently, autopilots were created and ultimately guidance laws were enacted. Various techniques have been discovered in this particular situation to choose the appropriate state estimation, guidance, and control algorithm to employ. These methods can be succinctly mentioned.

1.3.1 Review of state estimation studies

Firstly, a research introduces a new technique that utilizes a high-gain observer to accurately estimate the 3D water current velocities surrounding an AUV. The observer determines current velocities by comparing ground-measured vehicle velocities with model-based estimates. The utilization of real-time model identification guarantees the ongoing updating of the AUV model. The results demonstrate enhanced accuracy in current estimation compared to earlier methodologies, hence improving comprehension of the dynamics of underwater vehicles[17]. Another work presents a novel navigation approach designed specifically for AUVs by using the Unscented Kalman Filter (UKF). This approach provides improved precision in calculating vehicle velocity, which is vital for AUVs that operate without global positioning system (GPS) signals in underwater. The proposed technique has been effectively validated by experimental tests which are done during sea trials with Typhoon AUVs. These tests have shown promising results in accurately calculating vehicle dynamics for underwater exploration and surveillance missions [18]. Another study demonstrates cooperative localization and sea current estimate with numerous AUVs. To address the buildup of localization errors caused by sea currents, the study presents a navigation algorithm that allows numerous AUVs to estimate their navigation states while also estimating unknown sea currents. The approach combines the UKF with the linear Kalman filter [19]. Another research describes a reliable docking method for AUVs that can deal with unknown water currents. It assumes there is no onboard velocity sensor and utilizes a USBL mechanism to navigate to a stationary underwater docking station. An EKF calculates the water current and vehicle states [20]. Finally, a research describes a novel method for counteracting ocean currents in the navigation of AUVs. The method employs an EKF to estimate both the AUV state and water currents, which are then used in a modified heading controller to generate a current compensated desired heading [21]. A new study presents a novel UKF that is

specifically developed to accurately estimate the direction and magnitude of marine currents, as well as the navigation states of an AUV. The authors confirm this filter, which is an extension of a previously developed UKF, using data from onboard sensors of the MARTA AUV collected during sea trials [22].

1.3.2 Review of control law studies

First, many methods have been used to control AUVs. When these methods are examined, the following studies emerge. Firstly, a study introduces a disturbance observer-based model predictive control system for underactuated AUVs, dealing with unknown water current disturbances. By estimating the water current velocity component and external forces using a high-gain observer, a nonlinear model predictive controller is designed by taking into input constraints account [23]. A different study reveals a new Lyapunov-based model predictive control (LMPC) framework for the trajectory tracking of AUVs. It optimizes tracking performance while accounting for practical constraints such as actuator saturation and thrust allocation. The LMPC framework ensures stability with theoretical assurances and enhances robustness by adopting receding horizon implementation [24]. Another work utilizes robust sliding mode control for AUV, addressing modeling uncertainties and environmental disturbances. The proposed control theory demonstrates encouraging tracking performance in simulations with the actual AUV system [25]. Another study introduces an adaptive fuzzy sliding mode with a Proportional integral derivative (PID) sliding surface for depth control of an AUV. This approach addresses the chattering effect and enhances trajectory control through self-tuning techniques. The stability analysis confirms closed-loop dynamic stability, and simulations demonstrate improved tracking performance compared to traditional PID-based sliding mode control, especially in the presence of external disturbances [26]. Another work presents a robust control approach for process systems that include both stable and unstable outputs. It specifically deals with input limitations and control regions. The system employs a LQR to control system outputs and a robust MPC to control output setpoints. This guarantees that the outputs stay within their assigned zones and enforces restrictions on inputs. The simulation results on a simplified industrial process validate the effectiveness of the proposed technique [27]. A different study explores using cuckoo search to optimize weighted matrices in LQR controllers for AUVs. Cuckoo search efficiently discovers optimal matrices, improving the trajectory

tracking performance of AUVs [28]. A new study presents a detailed model and control approach for a hybrid AUV that takes into account both propelled and gliding modes of movement. An LQR is constructed and implemented on the nonlinear model using a linearization approach, which guarantees precise trajectory tracking even in the presence of underwater currents. The simulation results clearly show that the controller is highly effective, since it can autonomously switch to optimize both tracking error and energy usage [29]. Another study introduces a streamlined control technique for directing an AUV along a predetermined trajectory in three dimensions. The linear time-variant state-space model is obtained by linearizing the dynamics and kinematics model of the AUV's 6 degrees of freedom around the intended trajectory. Afterward, an LQR is formulated using this linear model and implemented on the nonlinear system to achieve trajectory tracking. The simulation findings validate the efficacy of the linear control method in several trajectory maneuvers, such as helical, saw-tooth, and 3D Dubin's route patterns [30]. Another study represents a control methodology for AUVs aimed at minimizing resistance in the vicinity of the ocean surface, where disturbances are more noticeable. A longitudinal resistance model is developed by using indicators such as pitch angle, heave displacement, driving energy, and additional resistance. An LQR controller, enhanced by the use of a genetic algorithm, is specifically designed to achieve stability in positioning and reduce energy usage. The simulation analysis validates the effectiveness of the proposed technique [31].

1.3.3 Review of guidance law studies

The previous sections of the thesis established the development of guidance algorithms to execute the path-following task. Upon examining the literature, various forms of these algorithms are observed. This section will provide a concise overview of various strategies. First of all, a study introduces a nonlinear adaptive line-of-sight path following controller for underactuated AUVs operating in ocean currents. First, it creates a new kinematic model to make it easier to build guidance laws. Second, it offers an adaptive guidance law that uses a current observer to change the vehicle's sideslip angle during curved-path following. The planned current observer ensures the indirect elimination of course angle inaccuracy [32]. Another work offers an unusual nonlinear ALOS guidance law for path following that may compensate for drift forces induced by external factors such as ocean currents. It operates similarly to classical

ILOS and adaptive ILOS guidance laws under virtually constant sideslip angles but outperforms them when adjusting for rapidly changing sideslip caused by time-varying disturbances. An input-to-state stable reduced-order extended state observer, known as the estimation of line of sight (ELOS) guidance law, is also added to calculate the LOS crab angle. The simulation results compare the performance of the ALOS, ILOS, and ELOS guidance laws under various scenarios with a Remus 100 AUV [33]. Another study presents two adaptive path-following controllers for marine crafts that use hydroacoustic relative velocity measurement. The first is an indirect adaptive controller that uses a disturbance observer to estimate and compensate for ocean currents, this is resulting in stability and precise drift estimates. The second is a direct adaptive integral line-of-sight controller that shows global convergence in the cross-track error. Both controllers are suitable for surface vessels and autonomous underwater vehicles [34]. Another control approach is developed for underactuated underwater vehicles to effectively navigate horizontal pathways in the presence of vertical ocean currents. The system incorporates the conventional LOS guidance law with integral action and utilizes three adaptive feedback controllers to effectively counteract disturbances. By simplifying the design challenge, it becomes possible to achieve an efficient path following horizontal straight-line trajectories, as confirmed by the results of simulations [35]. Another study presents a control method aimed at guiding underactuated marine surface vessels along predefined paths, even in the presence of ocean current disturbance. The traditional LOS guidance law is enhanced by incorporating integration action and utilizing adaptive feedback controllers to counteract environmental disturbances. By doing analysis, it is shown that this method guarantees a global asymptotic trajectory that follows straight routes, even when there are constant and non-rotational ocean currents [36].

1.4 Dissertation Overview

The general structure of the thesis can be explained as follows, chapter 1 is an introduction chapter, and in this chapter, the literature review and the scope of the study are mentioned. In Chapter 2, the dynamic model used and the developed sensor models are mentioned. In Chapter 3, state estimation and the design of EKF are mentioned. In Chapter 4, the controller developed is mentioned in detail. In Chapter 5, guidance laws developed are mentioned. In Chapter 6, the tests performed to test these

developed algorithms and the results obtained are mentioned. In the last chapter, chapter 7, the overall study is mentioned and the results obtained are mentioned.

2. DYNAMICAL MODEL OF REMUS-100

This part will cover the characteristics of the vehicle used, the dynamic model of the vehicle, and the derived sensor models.

2.1 Properties of Remus-100

The Remus-100 AUV, produced by Hydroid Inc., is the highest point in marine exploration technology, integrating state-of-the-art innovations with practical adaptability. The Remus-100 is specifically designed to operate autonomously and is highly proficient in a wide range of oceanographic tasks, including marine research and environmental monitoring. The modular design of the system enables easy integration of different sensors and payloads, allowing for customized configurations to fulfill specific mission goals. The Remus-100 showcases exceptional performance in underwater navigation, data collecting, and analysis, thanks to its advanced navigation systems and sensing technology. The modest size of this device guarantees its portability and convenience of use, allowing researchers and operators to initiate missions from various platforms such as research vessels, small boats, and even directly from shorelines. The Remus-100 is an essential tool for exploring and comprehending the intricacies of the ocean depths because of its wide range of uses in marine biology investigations, offshore infrastructure inspection, underwater mapping, and search and rescue operations [37].

Figure 2.1 : Remus-100 [37].

The dimensions of the REMUS-100 used in this study are given in Table 2.1 [37].

Table 2.1 : Dimensions of Remus-100 [37].

Dimensions of REMUS-100	
Diameter	19 cm
Weight	37 kg
Max Depth	100 m

The sensors of REMUS-100 used in this study is given in Table 2.2.

Table 2.2 : Sensors of Remus-100.

Sensor	Name	Description of Sensor
IMU	Inertial measurement unit	Measures angular velocity and acceleration
USBL	Ultra-short baseline	Measures position of AUV in inertial frame as x, y
DVL	Doppler velocity log	Measures body velocity components of AUV
Compass	Tilt and yaw compass	Measures pitch and yaw angle of AUV
DS	Depth sensor	Measures depth of AUV
STW Model	Speed through water (STW) measurement model	Measures speed through water of AUV

2.2 Dynamical Model of Remus-100

In this study, a dynamic model was not developed from scratch, an already-developed dynamic model was used. To briefly talk about this model, it is a Matlab function [38]. The inputs to the model are as follows: AUV's current states, current control inputs, sea current velocity, and sea current direction. This model outputs the time-dependent change of AUV states and the speed of the AUV. This situation can be easily seen in figure 2.2 below. In this figure, x represents states of AUV, x' represents time derivative of AUV states and U represents speed of AUV.

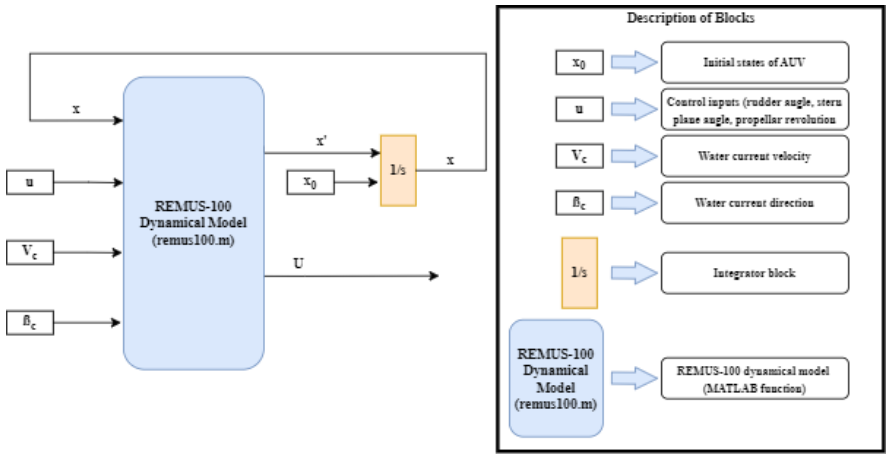

Figure 2.2 : Represenatation of dynamical model.

Below, the states of the dynamic model and the system inputs are shown, respectively.

$$x = \begin{vmatrix} u \\ v \\ w \\ p \\ q \\ r \\ x \\ y \\ z \\ \phi \\ \theta \\ \Psi \\ a_x \\ a_y \\ a_z \end{vmatrix} \tag{2.1}$$

$$u = \begin{vmatrix} \delta_r \\ \delta_s \\ n \end{vmatrix} \tag{2.2}$$

In the above equations, u, v, w respectively represent the body velocity components. The angular velocities of the AUV are denoted by p, q, r. The position of the AUV is indicated by x, y, z. The Euler angles of the AUV are denoted by ϕ, θ, Ψ. Acceleration components are also denoted by a_x, a_y, a_z. In addition, δ_r, δ_s, n represent rudder angle, stern plate angle and revolution of motor respectively.

2.3 Sensor Modelling

This section will address incorporating a sensor model to simulate the output of sensor data from state components that are outputs of the dynamic model. Dynamic model

outputs are regarded as the most accurate representation of real dynamic systems, in other words, they are called as ground truth. However, not all of these states can be directly measured and the available measurements are often subject to significant noise. Therefore, it is necessary to build sensor models that can effectively capture and monitor these noise effects in the dynamic model outputs. The primary cause for this can be elucidated as follows: For the algorithms to be utilized and evaluated in practical systems, they must be subjected to real-world settings.

When constructing the sensor model, a straightforward approach was employed. In summary, white noise was introduced to the dynamic model outputs to align with the sensor characteristics. By simulating a genuine test environment, the algorithms were subjected to more realistic conditions for testing.

Firstly, measurements of angular velocity and acceleration components will be defined as follows in equation 2.3, equation 2.4, equation 2.5, equation 2.6, equation 2.7 and equation 2.8.

$$a_{x_m} = a_x + N(0, \sigma_{acc}^2) + b_{acc} \tag{2.3}$$

$$a_{y_m} = a_y + N(0, \sigma_{acc}^2) + b_{acc} \tag{2.4}$$

$$a_{z_m} = a_z + N(0, \sigma_{acc}^2) + b_{acc} \tag{2.5}$$

$$p_m = p + N(0, \sigma_{gyro}^2) \tag{2.6}$$

$$q_m = q + N(0, \sigma_{gyro}^2) \tag{2.7}$$

$$r_m = r + N(0, \sigma_{gyro}^2) \tag{2.8}$$

$$\sigma_{acc} = 0.01\ m/s^2 \tag{2.9}$$

$$\sigma_{gyro} = 0.001\ rad/s \tag{2.10}$$

$$b_{acc} = 0.1\ m/s^2 \tag{2.11}$$

In above equations $a_x,\ a_y, a_z, p, q, r$ represent the states of dynamical model of Remus-100. $N(0, \sigma_{acc}^2)$ represents white gaussian noise with zero mean and variance of σ_{acc}^2. $a_{x_m}, a_{y_m}, a_{z_m}$ represent acceleration measurements that are the outputs of

accelerometer sensor model. p_m, q_m, r_m represent angular rate measurements that are the outputs of gyroscope sensor model. $N(0, \sigma_{gyro}^2)$ represents white gaussian noise with zero mean and variance of σ_{gyro}^2. σ_{acc} , σ_{gyro} represent standard deviation of measurements of accelerometer and gyroscope respectively. Finally, b_{acc} represents bias of accelerometer. In addition, these measurements are taken by IMU which consists of accelerometer and gyroscope.

Now, the measurements of position components which are taken by USBL and DS will be defined as follows in equation 2.12, equation 2.13 and equation 2.14.

$$x_m = x + N(0, \sigma_{USBL}^2) \tag{2.12}$$

$$y_m = y + N(0, \sigma_{USBL}^2) \tag{2.13}$$

$$z_m = z + N(0, \sigma_{DS}^2) \tag{2.14}$$

$$\sigma_{USBL} = 2\ m \tag{2.15}$$

$$\sigma_{DS} = 0.01\ m \tag{2.16}$$

In above equations x, y, z represent the position states of dynamical model of Remus-100. $N(0, \sigma_{USBL}^2)$ represents white gaussian noise with zero mean and variance of σ_{USBL}^2. $N(0, \sigma_{DS}^2)$ represents white gaussian noise with zero mean and variance of σ_{DS}^2. x_m, y_m, z_mrepresent position measurements that are the outputs of USBL and depth sensor model. $\sigma_{USBL}, \sigma_{DS}$ represent standard deviation of USBL and depth sensor measurements respectively.

In addition, the measurements of body velocity components which are measured by DVL will be defined as follows in equation 2.17, equation 2.18 and equation 2.19.

$$u_m = u + N(0, \sigma_{DVL}^2) \tag{2.17}$$

$$v_m = v + N(0, \sigma_{DVL}^2) \tag{2.18}$$

$$w_m = w + N(0, \sigma_{DVL}^2) \tag{2.19}$$

$$\sigma_{DVL} = 0.2\ m/s \tag{2.20}$$

In above equations u, v, w represent the body velocity states of dynamical model of Remus-100. $N(0, \sigma_{DVL}^2)$ represents white gaussian noise with zero mean and variance of σ_{DVL}^2. u_m, v_m, w_m represent body velocity measurements that are the outputs of DVL sensor model. σ_{DVL} represents standard deviation of DVL measurements.

Additionally, the measurements of pitch and yaw angle components which are measured by compass will be defined as follows in equation 2.21, equation 2.22.

$$\theta_m = \theta + N(0, \sigma_{compass}^2) \tag{2.21}$$

$$\Psi_m = \Psi + N(0, \sigma_{compass}^2) \tag{2.22}$$

$$\sigma_{compass} = 0.01\ rad \tag{2.23}$$

In above equations θ, Ψ represent the pitch and yaw angle states of dynamical model of Remus-100. $N(0, \sigma_{compass}^2)$ represents white gaussian noise with zero mean and variance of $\sigma_{compass}^2$. θ_m, Ψ_m represent pitch and yaw angle measurements that are the outputs of compass sensor model. $\sigma_{compass}$ represents standard deviation of compass measurements.

Finally, the measurement of STW component which are measured by STW model will be defined as follows in equation 2.24. As it is understood from equation 2.24, STW component are directly related to revolution per minute (RPM) value of propeller of AUV.

$$s_m = 0.001674521672131*\mathrm{RPM} + N(0, \sigma_{STW}^2) \tag{2.24}$$

$$\sigma_{STW} = 0.05\ m/s \tag{2.25}$$

In above equations s_m represents the measurement of STW component of Remus-100. $N(0, \sigma_{STW}^2)$ represents white gaussian noise with zero mean and variance of σ_{STW}^2. RPM represents revolution per minute value of propeller of AUV. σ_{STW} represents standard deviation of STW measurements. The correlation between RPM and STW is seen in Figure 2.3.

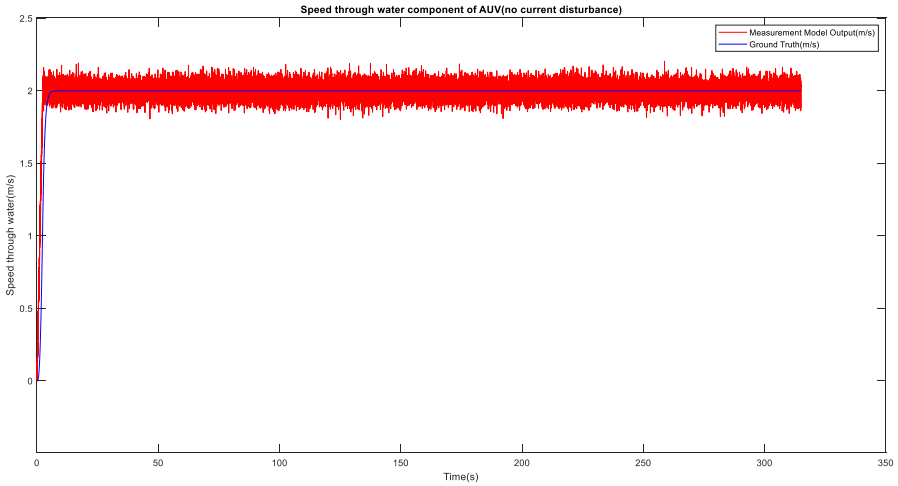

Figure 2.3 : Measurement model output and ground truth component of speed through water.

In Figure 2.3, the measurement model of speed through water and ground truth which is the speed of the AUV are seen easily. It concludes that the measurement model shows speed through water phenomena of the AUV reliably. This model output was obtained by testing with zero current disturbance and a constant commanded yaw angle.

3. STATE ESTIMATION OF REMUS-100

Initially, AUVs are employed in several sectors including military, defense, oil and gas exploration, underwater pipeline mapping, search operations for lost ships and airplanes, and investigation of underwater archaeological sites. These application domains encompass a significant issue that necessitates precise resolution. This issue is commonly referred to as localization or navigation. Navigation algorithms determine the precise location and orientation of the vehicle at any given moment. Furthermore, navigation serves as the input for the autopilots of underwater systems. In this particular context, it is crucial to precisely estimate and measure these inputs. As the autopilot relies on the vehicle's states and orientations as its reference values, these values must be accurately inputted into the autopilot. Furthermore, if an unmeasured state is to be utilized as an input for the autopilot, it is imperative to estimate this state. Furthermore, for the autopilot to create accurate outputs, it is necessary to eliminate noise from the measurement data produced by the sensor models. This can be achieved by the use of Kalman filters.

In addition, navigation in underwater vehicles poses challenges due to the inability of GPS waves to penetrate underwater. Therefore, it is imperative to devise an alternative solution in the absence of GPS. Various sensors, underwater acoustic positioning systems, and state estimation filters such as EKF, UKF, and Particle Filters can be used to estimate the system states of the underwater vehicles. Furthermore, these vehicles are subjected to current disturbance while operating underwater. This disturbance can pose significant challenges in docking operations where precise positioning is crucial, as well as in military applications or long-term missions like mapping. This study presents a solution approach to the topic at hand. The position components, velocity components, acceleration components, Euler angles, angular rates, and sea current components of the AUV will be estimated. The sensors to be utilized for these estimations include USBL, IMU, compass, and DVL. The Extended Kalman filter will be employed as the estimating technique because of its suitability for nonlinear systems, high accuracy of estimation, adaptability, and simplicity.

3.1 Extended Kalman Filter

In this section, EKF will be mentioned and how this filter is used in this study. EKF is widely used for estimating the state in a range of industries, such as robotics, aircraft, and autonomous vehicles. The main goal of state estimation is to deduce the internal state of a dynamic system using sensor measurements that may contain noise, as well as potentially incomplete information of the system's dynamics. EKF achieves exceptional performance in this task by the iterative estimation of the system's state, employing a combination of prediction and update processes. EKF is used in state estimation applications to represent the system's evolution over time using a series of nonlinear equations, typically derived from physical laws or dynamic models. Subsequently, they integrate disruptive sensor measurements to revise the state estimations, progressively enhancing the prediction and augmenting their accuracy as time progresses. The iterative nature of this process allows the EKF to generate reliable and precise estimates of the system's state, even when there are uncertainties and sensor noise present. Consequently, the Extended Kalman Filter is extensively employed in various fields, including satellite navigation and localization and mapping in mobile robots. In these applications, accurate state estimation is essential for autonomous operation.

3.1.1 Estimation procedure of EKF

EKF algorithm comprises two primary components, namely the prediction stage and the update stage. The equations for each of these stages will be provided in the order they are mentioned[39].

$$\hat{x}_k^- = f_{k-1}(\hat{x}_{k-1}^+, u_{k-1}, 0) \tag{3.1}$$

$$P_k^- = F_{k-1}P_{k-1}^+F_{k-1}^T + L_{k-1}Q_{k-1}L_{k-1}^T \tag{3.2}$$

The prediction stage can be represented by the processes in equation 3.1 and equation 3.2. $\hat{x}_{k-1}^+$ represents previous state estimation, $\hat{x}_k^-$represents state prediction, u_{k-1} represents model input, f_{k-1} system evolution equation. P_k^- represents state covariance prediction, F_{k-1} represents process model Jacobian matrix, P_{k-1}^+ represents previous state covariance estimation, L_{k-1} represents process noise model Jacobian matrix, Q_{k-1} represents covariance matrix of the process noise. The update stage can be

represented by the processes in equation 3.3, equation 3.4, equation 3.5, equation 3.6 and equation 3.7.

$$H_k = \frac{\partial h_k}{\partial x}\Big|_{\hat{x}_k^-} \tag{3.3}$$

$$M_k = \frac{\partial h_k}{\partial v}\Big|_{\hat{x}_k^-} \tag{3.4}$$

$$K_k = P_k^- H_k^T (H_k P_k^- H_k^T + M_k R_k M_k^T)^{-1} \tag{3.5}$$

$$\hat{x}_k^+ = \hat{x}_k^- + K_k\left[y_k - h_k(\hat{x}_k^-, 0)\right)\Big] \tag{3.6}$$

$$P_k^+ = (I - K_k H_k) P_k^- \tag{3.7}$$

H_k represents Jacobin matrix of the measurement function, M_k represents Jacobian matrix of the measurement noise function, R_k represents covariance matrix of measurement noise, K_k represents Kalman gain. $\hat{x}_k^+$ represents state update, y_k represents measurement vector, h_k represents measurement function. P_k^+ represents state covariance update and I represents identity matrix.

3.1.2 Estimated states

Firstly, there are 14 states that will be estimated by EKF in this study. These states can be seen as follow.

$$\hat{x} = \begin{vmatrix} E \\ N \\ s \\ \phi \\ \theta \\ \Psi \\ C_E \\ C_N \\ u \\ v \\ a_x \\ a_y \\ b \\ r \end{vmatrix} \tag{3.8}$$

In above equation, $\hat{x}$ represents estimated states, E, N represent east and north position respectively, s represents speed through water, ϕ, θ, Ψ represent roll, pitch and yaw

angle respectively, C_E, C_N represent sea current velocity component through east and north direction respectively. u, v represent body velocity component with respect to x and y axis respectively. a_x, a_y represent acceleration component with respect to x and y axis respectively, b represents accelerometer bias and r represents yaw rate component of AUV.

3.1.3 Detailed design of EKF

Now, the details of state estimation with EKF will be given. Firstly, state prediction equations were determined as follows.

$$E_{(k)} = E_{(k-1)} + s_{(k-1)} \cdot \sin\left(\psi_{(k-1)}\right) \cdot \Delta t + C_{E_{(k-1)}} \cdot \Delta t \tag{3.9}$$

$$N_{(k)} = N_{(k-1)} + s_{(k-1)} \cdot \cos\left(\psi_{(k-1)}\right)\Delta t + C_{N_{(k-1)}} \cdot \Delta t \tag{3.10}$$

$$s_{(k)} = s_{(k-1)} \tag{3.11}$$

$$\emptyset_{(k)} = \emptyset_{(k-1)} + \begin{pmatrix} \tilde{p} + \tilde{q} \cdot \sin\left(\emptyset_{(k-1)}\right) \cdot \tan\left(\theta_{(k-1)}\right) + \\ \tilde{r} \cdot \cos\left(\emptyset_{(k-1)}\right) \cdot \tan\left(\theta_{(k-1)}\right) \end{pmatrix} \Delta t \tag{3.12}$$

$$\theta_{(k)} = \theta_{(k-1)} + \left(\tilde{q} \cdot \cos\left(\emptyset_{(k-1)}\right) - \tilde{r} \cdot \sin\left(\emptyset_{(k-1)}\right)\right) \Delta t \tag{3.13}$$

$$\psi_{(k)} = \psi_{(k-1)} + \left(\tilde{q} \cdot \frac{\sin\left(\emptyset_{(k-1)}\right)}{\cos\left(\theta_{(k-1)}\right)} + \tilde{r} \cdot \frac{\cos\left(\emptyset_{(k-1)}\right)}{\cos\left(\theta_{(k-1)}\right)}\right) \Delta t \tag{3.14}$$

$$C_{E_{(k)}} = C_{E_{(k-1)}} \tag{3.15}$$

$$C_{N_{(k)}} = C_{N_{(k-1)}} \tag{3.16}$$

$$u_{(k)} = u_{(k-1)} + a_{x_{(k-1)}} \cdot \Delta t \tag{3.17}$$

$$v_{(k)} = v_{(k-1)} + a_{y_{(k-1)}} \Delta t \tag{3.18}$$

$$a_{x_{(k)}} = a_{x_{(k-1)}} \tag{3.19}$$

$$a_{y_{(k)}} = a_{y_{(k-1)}} \tag{3.20}$$

$$b_{(k)} = b_{(k-1)} \tag{3.21}$$

$$r_{(k)} = r_{(k-1)} \tag{3.22}$$

Equation 3.9 and equation 3.10 represent state prediction equations of North-East position states. Δt represents time step for whole simulation, which is 0.01 second. Equation 3.11 represents state prediction equation for STW. Equation 3.12, equation 3.13 and equation 3.14 represent the state prediction equations for Euler angles states of AUV. $\tilde{p}, \tilde{q}, \tilde{r}$ represent roll, pitch and yaw rate measurements and these are u_{k-1} components that was defined in equation 3.1. Equation 3.15 and equation 3.16 represent the state prediction equations for sea current estimation. Equation 3.17 and equation 3.18 represent the state prediction equations for body velocity component of AUV. Equation 3.19, equation 3.20 and equation 3.21 represent the state prediction equations for acceleration and accelerometer bias. Finally, equation 3.22 represents the state prediction equation for yaw rate estimation.

Now, initial state estimation x, initial state covariance P matrix, state covariance matrix of the process noise Q matrix and covariance matrix of measurement noise R will be defined as follows.

$$x = \begin{vmatrix} 0 \\ 0 \\ 0.6 \\ 0 \\ 0 \\ 0 \\ 0 \\ 0 \\ 0 \\ 0 \\ 0 \\ 0 \\ 0 \\ 0 \end{vmatrix} \tag{3.23}$$

$$P = diag(100,100, 2.25, 1.6 * 10^{-3}, \quad 1.6 * 10^{-5}, \\ 0.16, 0.1, 0.1, 0.1, 0.10, 1, 1, 1, 0.0001) \tag{3.24}$$

$$Q = diag(2.5 * 10^{-7}, 2.5 * 10^{-7}, 10^{-6}, 10^{-8}, 2.5 * 10^{-9}, \tag{3.25}$$

$$2.5 * 10^{-9}, 10^{-8}, 10^{-8}, 2.5 * 10^{-7}, 2.5 * 10^{-7}, 2.5 * 10^{-9},$$
$$2.5 * 10^{-9}, 4, 2.5 * 10^{-7})$$

$$R = diag(200, 200, 0.0125, 0.001, \quad 0.001, \quad 8, 8, 0.0010, 0.0010, 0.000010) \tag{3.26}$$

In above, the initial state estimate is represented in equation 3.23, the initial state covariance is represented in equation 3.24, the process noise covariance is represented in equation 3.25 and the measurement noise covariance is represented in equation 3.26. Finally, "diag" keyword is used to define diagonal matrix, since these matrices are 14x14 diagonal matrices.

All equations have been given so far and the details of the prediction stage have also been mentioned. The measurement data used in the prediction stage was only the angular rate data measured from the gyroscope. In the update stage, data produced by other sensors will be used. Now, the update stage will be briefly mentioned and then the state estimation test scenario and results will be mentioned. The measurements that were used in update stage can be seen below.

$$y = \begin{vmatrix} E \\ N \\ s \\ \theta \\ \Psi \\ u \\ v \\ a_x \\ a_y \\ r \end{vmatrix} \tag{3.27}$$

In equation 3.27, the measurement vector y is seen. E, N are measured by USBL, s is measured by STW model. θ, Ψ are measured by compass and u, v are measured by DVL. Finally, a_x, a_y, r are measured by IMU. Thus, all measurement components used in the update stage are obtained. Afterwards, the H matrix defined in the EKF equations will be defined as below.

The size of H matrix will be 10x14 since there are 10 measurements and 14 states. Additionally, H matrix was obtained by finding Jacobian matrix of measurement function as defined in equation 3.3. This matrix can be seen in equation 3.28 below.

$$H = \begin{bmatrix} 1 & 0 & 0 & 0 & 0 & 0 & 0 & 0 & 0 & 0 & 0 & 0 & 0 \\ 0 & 1 & 0 & 0 & 0 & 0 & 0 & 0 & 0 & 0 & 0 & 0 & 0 \\ 0 & 0 & 1 & 0 & 0 & 0 & 0 & 0 & 0 & 0 & 0 & 0 & 0 \\ 0 & 0 & 0 & 0 & 1 & 0 & 0 & 0 & 0 & 0 & 0 & 0 & 0 \\ 0 & 0 & 0 & 0 & 0 & 1 & 0 & 0 & 0 & 0 & 0 & 0 & 0 \\ 0 & 0 & 0 & 0 & 0 & 0 & 0 & 0 & 1 & 0 & 0 & 0 & 0 \\ 0 & 0 & 0 & 0 & 0 & 0 & 0 & 0 & 0 & 1 & 0 & 0 & 0 \\ 0 & 0 & 0 & 0 & 0 & 0 & 0 & 0 & 0 & 0 & 1 & 0 & 1 & 0 \\ 0 & 0 & 0 & 0 & 0 & 0 & 0 & 0 & 0 & 0 & 0 & 1 & 1 & 0 \\ 0 & 0 & 0 & 0 & 0 & 0 & 0 & 0 & 0 & 0 & 0 & 0 & 0 & 1 \end{bmatrix} \tag{3.28}$$

As a result, all EKF equations have been explained so far and the contents of the matrices in the equations have been mentioned in detail. In the last section, testing of the EKF algorithm and the obtained states will be mentioned.

3.1.4 State estimation results

In this section, testing of the EKF algorithm and the obtained states will be discussed. First, it is necessary to briefly mention the scenario in which EKF was tested. In the figure below, it is simply seen how an AUV moves when it is not exposed to the current and when it is exposed to the current, these two paths are scenarios in which the AUV is controlled by giving a fixed yaw command.

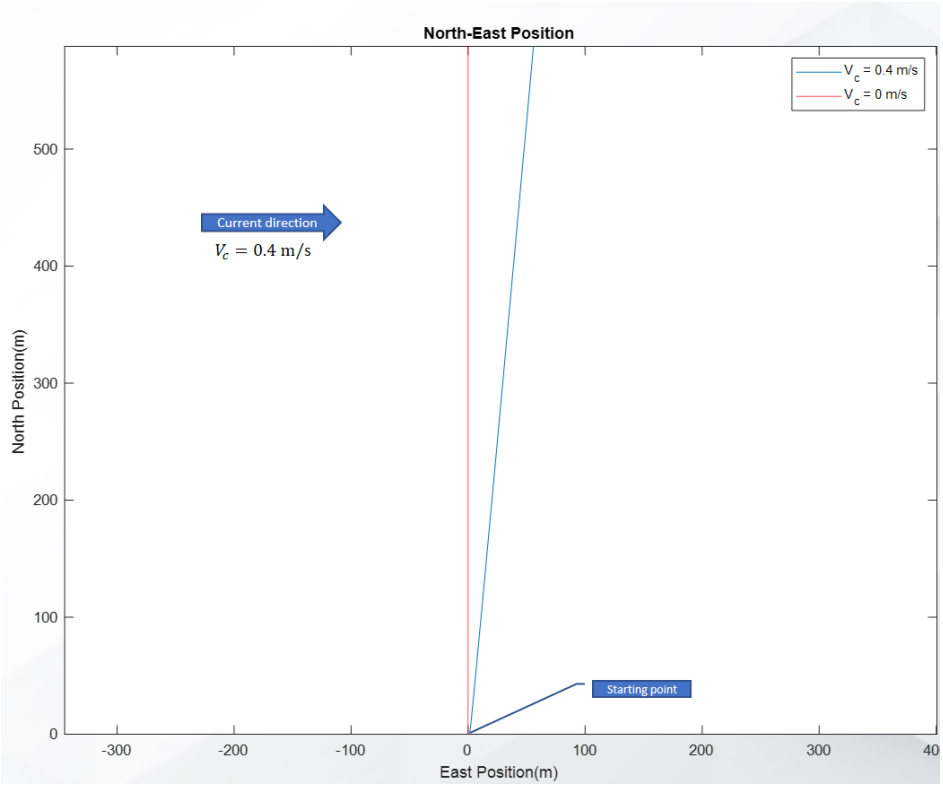

Figure 3.1 : Testing scenario for EKF design.

The following figures are estimations of the states of the AUV exposed to 0.4 m/s sea current. These state estimations are the outputs of EKF. First, position estimations of AUV can be seen in figure 3.2 below.

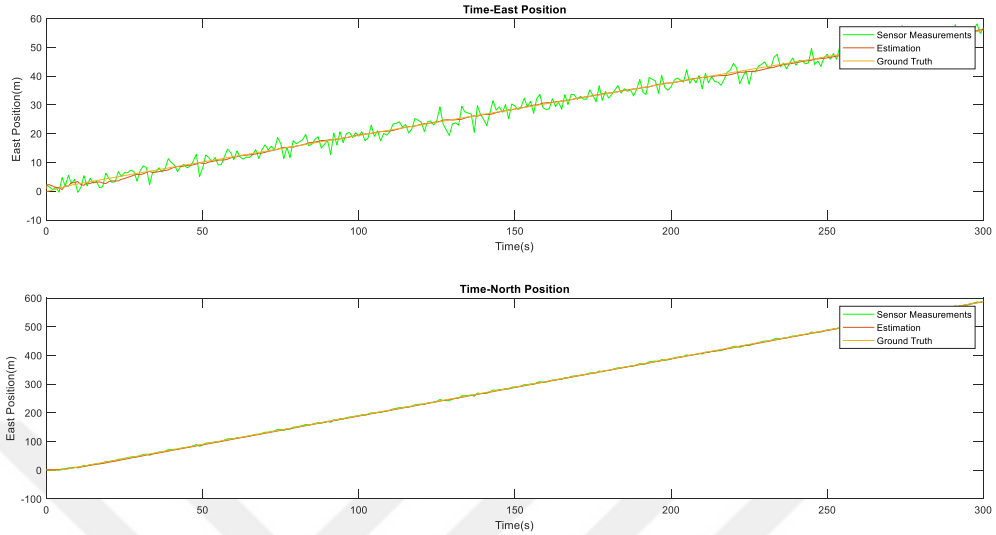

Figure 3.2 : Position estimations of AUV.

In figure 3.2, the position estimation, sensor measurements of USBL and ground truth which is output of dynamical model can be seen. Position estimations were used in guidance algorithms as input, therefore, these quantities must be estimated well. When the figure is examined, it can be seen that the noise of the sensor measurements of USBL has been significantly reduced. In this case, it shows that EKF fulfilled its duty. The other state that was estimated is STW, the STW estimations of AUV can be seen in figure 3.3 below.

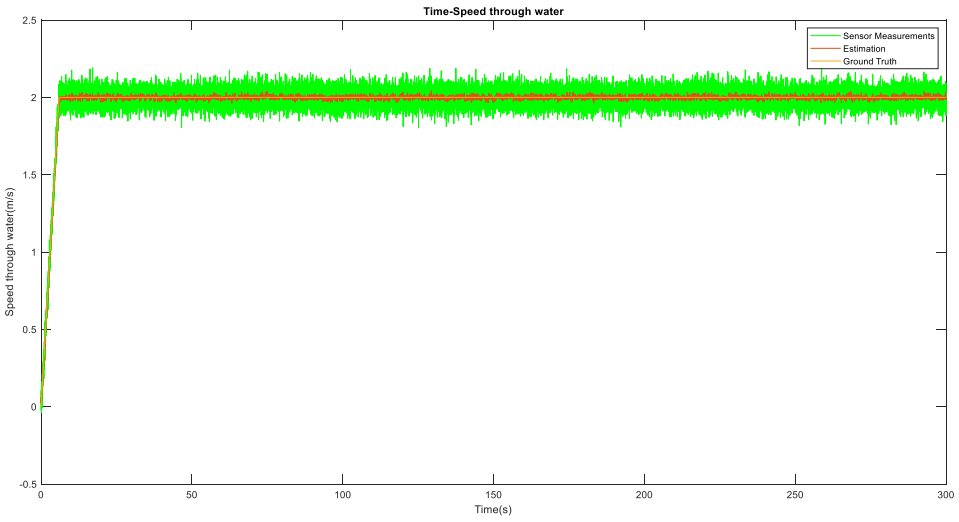

Figure 3.3 : Speed through water estimation.

In figure 3.3, the STW estimation, measurement and ground truth which is output of sensor model are shown. STW estimations are used in position estimation as well in EKF, therefore, this must be estimated well. When the figure is examined, it can be seen that the noise of the sensor model of STW has been significantly reduced. In addition, Euler angles were estimated and these estimations of AUV can be seen in figure 3.4 below.

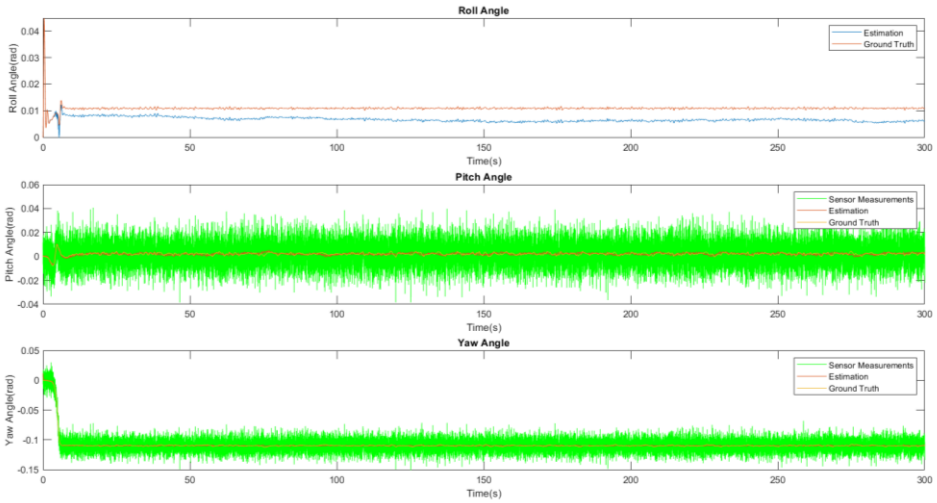

Figure 3.4 : Euler angles estimations.

In figure 3.4, the roll, pitch and yaw angle estimations, measurements and ground truth components which are the output of dynamical model are shown. Euler angle estimations were used in autopilots as input, therefore, these must be estimated well. When the figure is examined, it can be seen that the roll angle is estimated very well although the roll angle was not measured directly, it was estimated quite well even with the data taken from the gyroscope. since there is no measurement update for roll angle has been significantly reduced. In addition, when the estimations of other Euler angles are examined, the measurements of the pitch angle and yaw angle are quite noisy data, if these were fed directly as input to the autopilots, the autopilots could be led to instability. However, when the estimations with EKF output are examined, it is seen that the estimations are free from sensor noise and are quite similar to ground truth. In this case, these outputs can be easily used on autopilot. In this case, it can be concluded that EKF has fulfilled its expected duty. In addition, current velocity components were estimated and these estimations of AUV can be seen in figure 3.5 below.

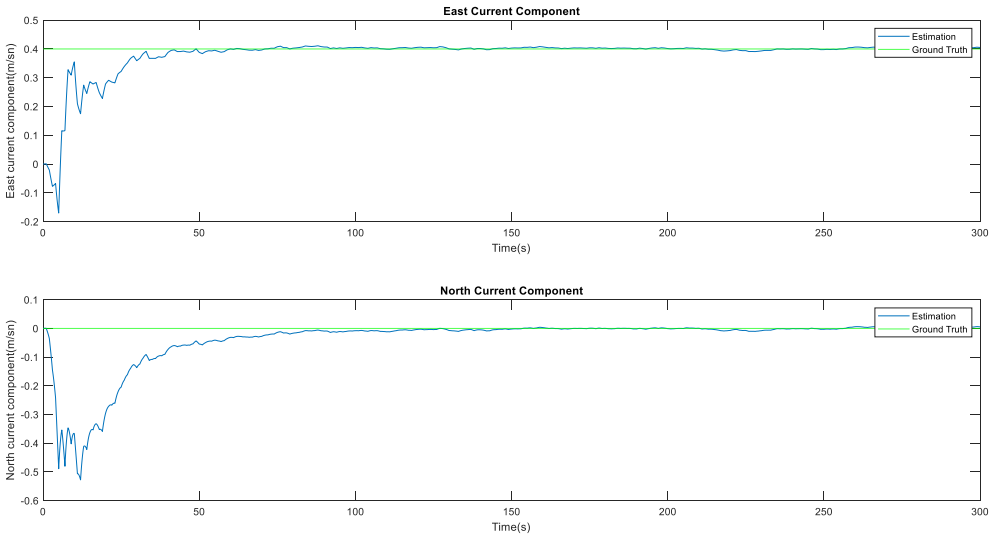

Figure 3.5 : Current velocity estimations.

In figure 3.5, the current velocity components estimation and ground truths can be seen. When the figure is examined, it can be concluded that the current velocity estimation process has been successfully completed and the estimation results are quite similar to ground truth. In addition, body velocity components were estimated and these estimations of AUV can be seen in figure 3.6 below.

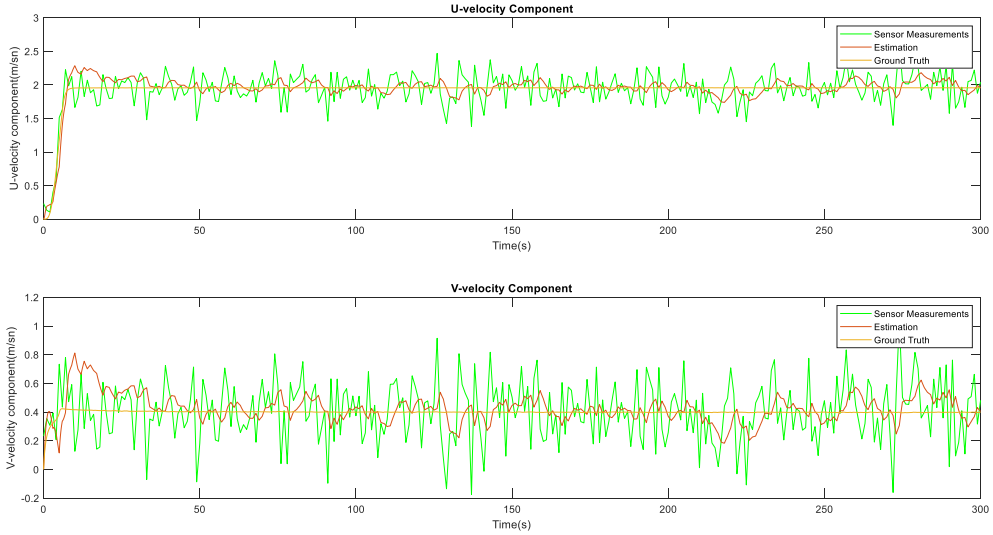

Figure 3.6 : Estimation of body velocity components.

In figure 3.6, body velocity estimations, measurements and ground truth components which are the output of dynamical model are shown. When the figure is examined, it can be concluded that the body velocity estimation process has been completed successfully, because the resulting estimation outputs have less noise than sensor

measurements, and these estimation results are quite similar to ground truth. Additionally, acceleration components and bias were estimated and these estimations can be seen in figure 3.7 below.

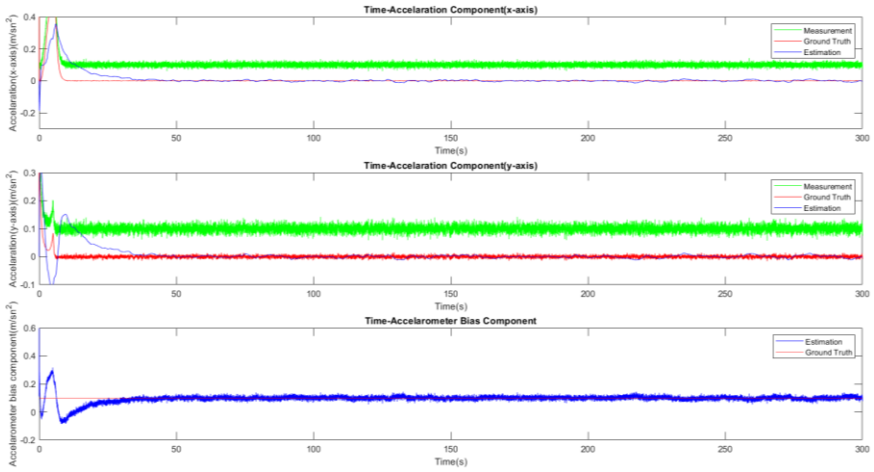

Figure 3.7 : Estimation of accelaration and bias components.

In figure 3.7, acceleration and bias estimations, measurements and ground truth components which are the output of dynamical model are shown. When the figure is examined, it can be concluded that the acceleration and bias estimation process has been completed successfully, because the resulting estimation outputs have less noise than the sensor measurements, and these estimation results are quite similar to ground truth. Additionally, the sensor bias has been estimated very well. Finally, yaw rate was estimated and this estimation can be seen in figure 3.8 below.

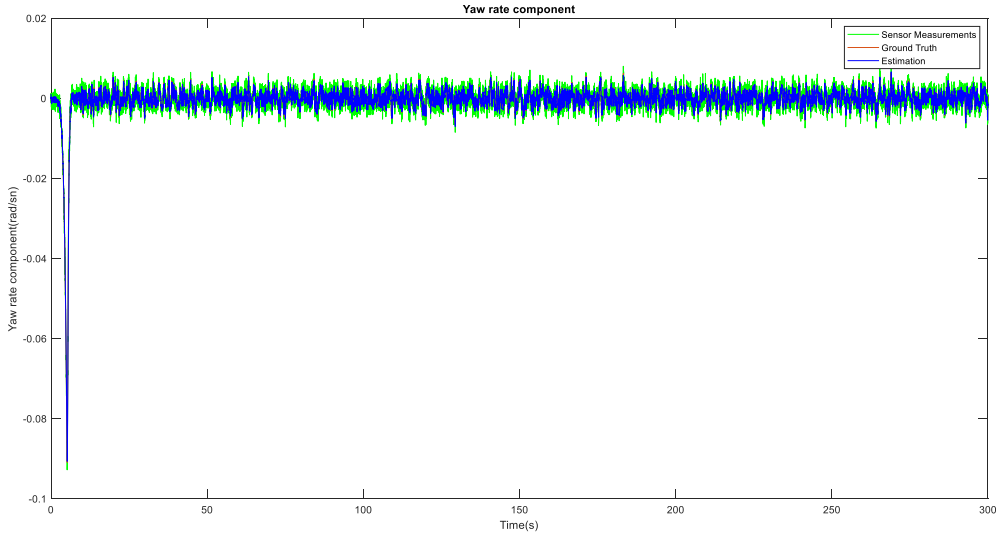

Figure 3.8 : Estimation of yaw rate.

In figure 3.8, yaw rate estimation, measurement and ground truth component which is the output of dynamical model are shown. When the figure is examined, it can be concluded that the yaw rate estimation process has been completed successfully, because the resulting estimation output has less noise than the sensor measurement.

As a result, the inputs to be used in autopilot and guidance were estimated using EKF. In this way, the realism of the study is increased, because, in real-life problems, there are unmeasurable states of the AUV, and the measurable states are already quite noisy. Thanks to EKF, unknown states are estimated and noise levels are reduced in known state measurements.

Now, the performance of EKF's estimations will be examined in more detail. In this context, the diagonal elements of the P matrix, which is the state estimation covariance matrix, will be examined. In order to understand that EKF performs proper estimation, we need to see that these covariance elements converge to a certain value after a certain period of time. In addition, the state estimation error must remain between these covariance values. In other words, standard deviations are obtained by taking the square root of the covariance elements obtained from the diagonal elements of the P matrix. Afterwards, it will be seen that the state estimation error is between ±3 times these standard deviations. As a result, if the state estimation error falls between this ±3σ channel, it is concluded that EKF performs well when estimating good states. Figure 3.9 shows the ±3σ channel obtained from state covariance matrix P and position estimation error.

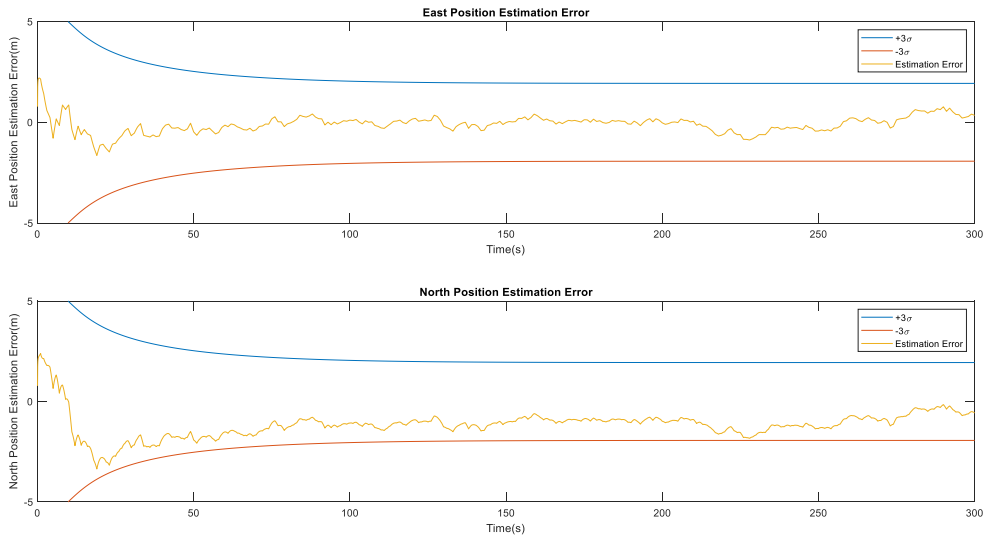

Figure 3.9 : Position estimation error.

It can be seen in Figure 3.9 that the position estimation error remains within the ±3σ channel and it is also seen that the P matrix element converges to a certain value stably. This means that the state estimation is done properly. Figure 3.10 shows the ±3σ channel obtained from state covariance matrix P and speed through water estimation error.

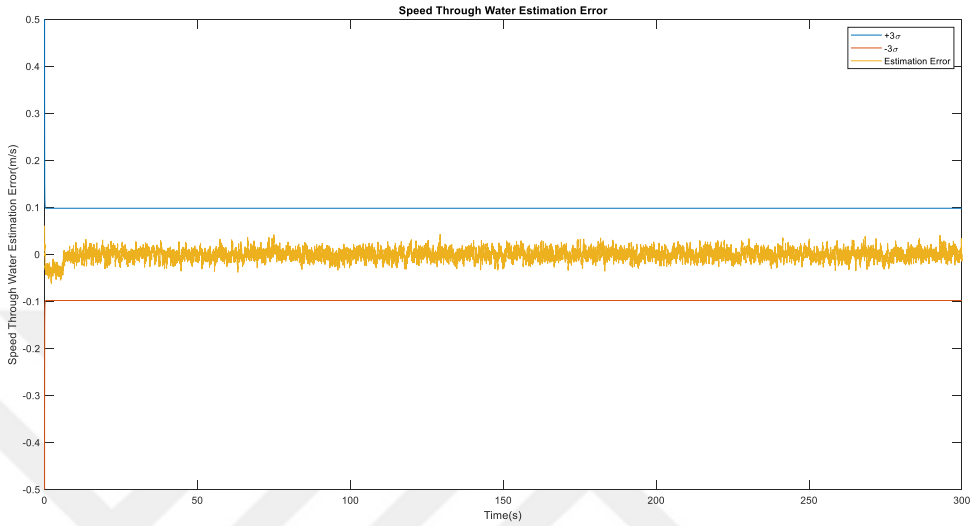

Figure 3.10 : Speed through water estimation error.

It can be seen in Figure 3.10 that the speed through water estimation error remains within the ±3σ channel during its whole operation and it is also seen that the related P matrix element converges to a certain value. This means that the state estimation is done properly. Figure 3.11 shows the ±3σ channel obtained from state covariance matrix and Euler angles estimation error.

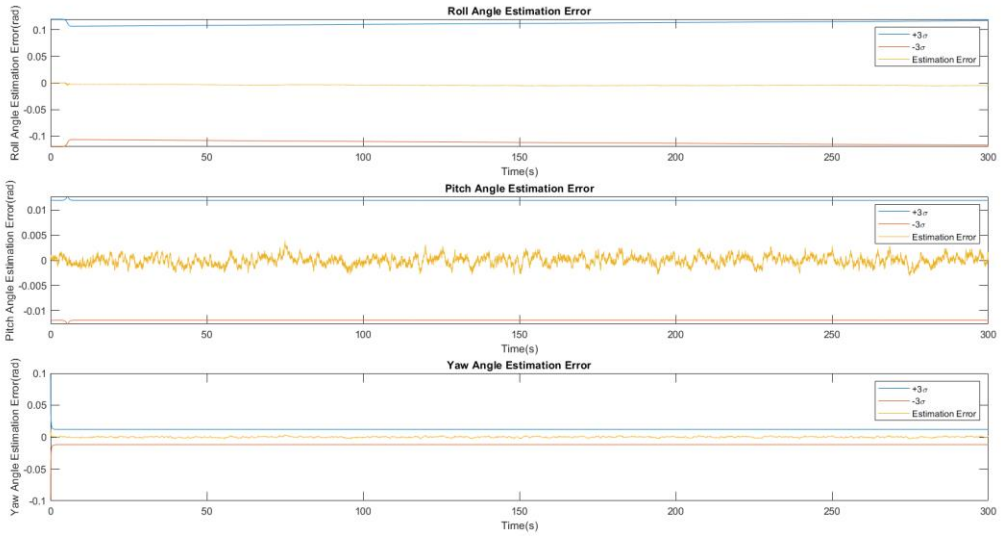

Figure 3.11 : Euler angles estimation error.

It can be seen in Figure 3.11 that the Euler angle estimation error remains within the ±3σ channel and it is also seen that the P matrix element converges to a certain value. This means that the state estimation is done properly. Figure 3.12 shows the ±3σ channel obtained from state covariance matrix P and current components estimation error.

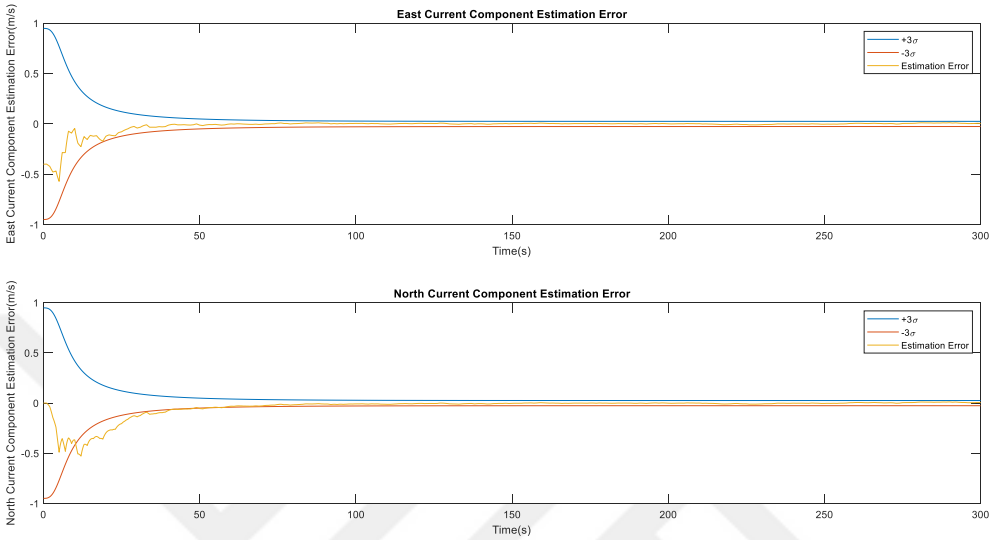

Figure 3.12 : Current components estimation error.

It can be seen in Figure 3.12 that the current components estimation error remains within the ±3σ channel and it is also seen that the P matrix element converges to a certain value. This means that the state estimation of current components is done properly. Figure 3.13 shows the ±3σ channel obtained from state covariance matrix and body velocity estimation error.

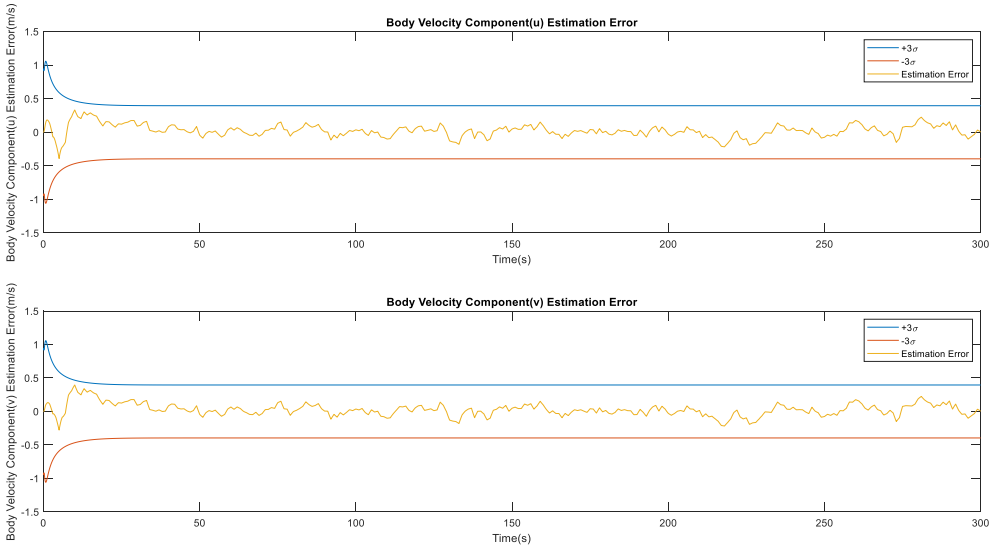

Figure 3.13 : Body velocity estimation error.

It can be seen in Figure 3.13 that the body velocity estimation error remains within the ±3σ channel and it is also seen that the P matrix element converges to a certain value. This means that the state estimation is done properly. Figure 3.14 shows the ±3σ channel obtained from state covariance matrix, acceleration and bias estimation error.

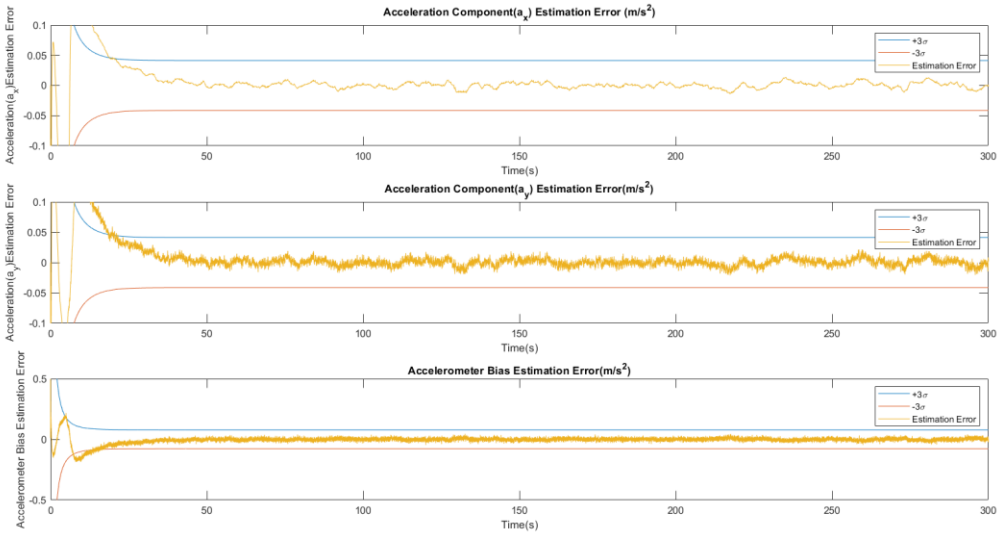

Figure 3.14 : Accelaration and bias estimation error.

It can be seen in Figure 3.14 that the acceleration and bias estimation error remains within the ±3σ channel and it is also seen that the P matrix element converges to a certain value. This means that the state estimation is done properly. Figure 3.15 shows the ±3σ channel obtained from state covariance matrix P, yaw rate estimation error.

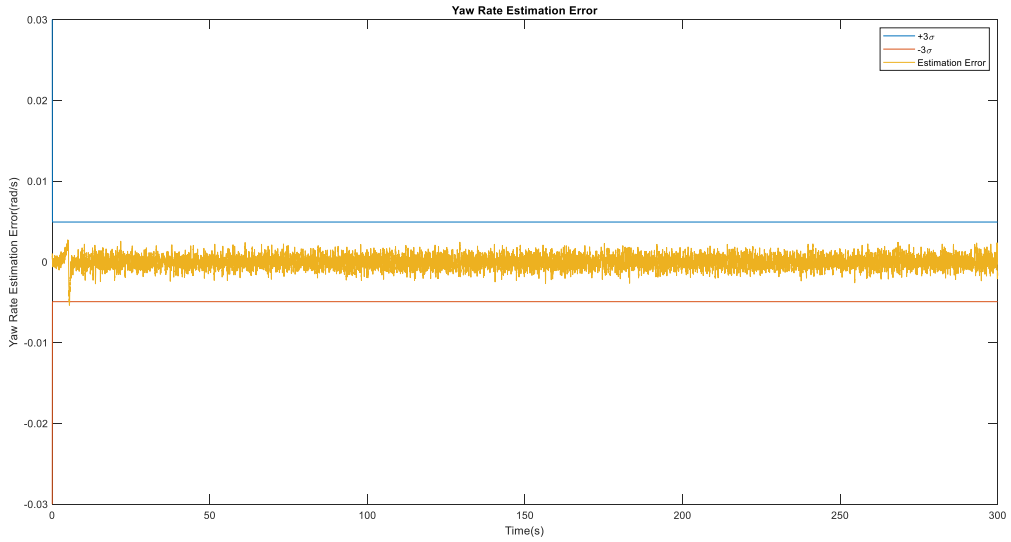

Figure 3.15 : Yaw rate estimation error.

It can be seen in Figure 3.15 that the yaw rate estimation error remains within the ±3σ channel and it is also seen that the P matrix element converges to a certain value. This means that the state estimation is done properly. As a result, state estimation results have been mentioned so far. The errors of the state estimations were calculated, while calculating these errors, the ground truth values were subtracted from the estimation value, and in this way, how many errors were made in the estimation process was calculated. Additionally, the relationship between the estimation error and the standard deviation channels obtained from the state covariance matrix was shown. In addition, it was observed that the values of the state covariance matrix converged to a certain value for each element. With these results, it was seen that EKF was working stably.

4. CONTROL OF REMUS-100

In this chapter, the controllers developed in this study will be mentioned. First, the LQR controller was used as the final controller. In this context, the development process, methodology and testing process of the controller will be mentioned in the following subchapters.

4.1 Linear Quadratic Regulator

LQR control is a prevalent method in control systems engineering that is employed to create optimal feedback controllers for linear dynamic systems. The main goal of LQR control is to minimize a quadratic cost function that captures the system's performance requirements, such as control effort and state variances, over a finite or infinite time period. LQR control integrates optimal control theory with linear system dynamics to calculate control inputs optimizing system performance while adhering to prescribed restrictions. The basis of LQR control is rooted in the Linear Quadratic Regulator problem, which entails solving a system of coupled differential Riccati equations to ascertain the ideal state feedback gain matrix. The gain matrix determines the control strategy that minimizes the cost function while guaranteeing the stability and resilience of the closed-loop system. LQR control offers a systematic approach to creating optimal controllers using mathematical optimization concepts, in contrast to classic control systems like PID control which rely on heuristic modifying of control parameters. The LQR control algorithm is utilized in a wide range of industries, such as aerospace, automotive, robotics, and process control. Its primary purpose is to accurately regulate the dynamics of a system in order to achieve certain performance goals. The efficacy of this system is derived from its capability to manage intricate systems with multiple variables and adjust to evolving operating conditions using online parameter estimates and model predictive control methodologies. As a result, LQR controllers are a powerful tool for controlling dynamical systems. They are relatively easy to design and implement, and they can provide good performance in a variety of applications.

4.1.1 Theory of linear quadratic regulator

LQR controller is a fundamental approach in optimal control theory designed specifically for linear time-invariant (LTI) systems described by state-space representations defined in the equations below.

$$\dot{x}(t) = Ax(t) + Bu(t) \tag{4.1}$$

$$y(t) = Cx(t) + Du(t) \tag{4.2}$$

In equation 4.1, $x(t)$ represents state vector, $u(t)$ represents control input, A represents state transition matrix, B represents input matrix. In equation 4.2, $y(t)$ represents output vector, C represents output matrix and D represents direct transition matrix.

LQR is a control technique that creates feedback control laws that minimize a quadratic cost function. This cost function is a combination of the state and control input trajectories over a specific time, which can be either finite or infinite. The LQR problem formulation centers on minimizing the subsequent cost function [40].

$$J = \int_0^\infty (x^T Q x + u^T R u) dt \tag{4.3}$$

In equation 4.3, Q and R are positive semi-definite weighting matrices that indicate the relative significance of state deviation and control attempts, correspondingly. The optimal feedback control law for the LQR problem is obtained by solving the corresponding algebraic Riccati equation as shown below [40].

$$A^T P + PA - PBR^{-1}B^T P + Q = 0 \tag{4.4}$$

In equation 4.4, the matrix P represents the solution matrix that is both symmetric and positive definite. It is commonly known as the state feedback gain matrix. The matrix P represents the ideal trade-off between state regulation and minimizing control effort. It determines the feedback control rule as shown in equation 4.5 and equation 4.6 below [40].

$$K = R^{-1}B^T P \tag{4.5}$$

$$u = -Kx \tag{4.6}$$

In equation 4.5 and equation 4.6, K represents feedback control gain, u represents control input, x represents the system state. It is important to emphasize that LQR is intrinsically connected to the ideas of linear system theory, requiring the underlying dynamical system to be both linear and time-invariant. Linearization around operational points is required to implement LQR techniques in nonlinear systems. To summarize, LQR provides a comprehensive mathematical foundation for designing feedback controllers that optimize system performance while meeting strict stability and control cost requirements.

4.1.2 Design procedure of linear quadratic regulator

First, the nonlinear model of the Remus-100 AUV is used in this study, but the LQR control technique is a controller technique that can be applied to linear systems. Therefore, the system needs to be linearized. This linearization will be done along the given path throughout the entire operation of the AUV. Numerical linearization technique was used as the linearization technique. In detail, A and B matrices were obtained with first order Taylor expansion as described as follows [41].

Firstly, this numerical linearization technique can be applied to any nonlinear model, especially this approach is used in aircrafts to linearize the aircraft model. The explicit state equations in equation 4.7 can be expanded using a multivariate Taylor series around the point (x_e, u_e) which are equilibrium point or trim point in equation 4.8.

$$\dot{x}(t) = f(x(t), u(t)) \tag{4.7}$$

$$\dot{x} + \delta\dot{x} = f(x_e, u_e) + \frac{\partial f}{\partial x}\delta x + \frac{\partial f}{\partial u}\delta u + \text{h.o.t.} \tag{4.8}$$

In equation 4.8, the partial derivative terms represent Jacobian matrices such as $\frac{\partial f}{\partial x}$ and perturbations such as δx. Also, h.o.t. represents higher order terms that will be ignored.

$$\delta x \equiv (x - x_e) \tag{4.9}$$

$$\delta u \equiv (u - u_e) \tag{4.10}$$

In equation 4.9 and 4.10, the terms $\delta x, \delta u$ are very small. As it is stated earlier that (x_e, u_e) are equilibrium points, then the equation 4.11 is obtained.

$$0 = \dot{x} = f(x_e, u_e) \tag{4.11}$$

$$\delta \dot{x} = \frac{\partial f}{\partial x}\delta x + \frac{\partial f}{\partial u}\delta u \tag{4.12}$$

Equation 4.12 is expressed in the form of the Linear Time-Invariant (LTI) state equation.

$$\dot{x} = Ax + Bu \tag{4.13}$$

In equation 4.13, x, u represent perturbation from the equilibrium point. However, $\dot{x}$ represents precise value of the derivative vector. With the obtained equation form, Remus-100 may achieve vehicle linearization even during cruising. The dynamic model outputs provide information about the changes in the states over time, which can be used to linearize the system.

Next, the initial partial derivatives must be estimated, which form the Jacobian matrices. The technique of estimating will be demonstrated using a function that involves only one variable, z, which is equal to $g(v)$. By employing Taylor series expansions of function g around the point $v = v_e$, these are obtained as follows.

$$z_1 \equiv g(v_e + h) = g(v_e) + h\frac{\partial g}{\partial v}(v_e) + \frac{h^2}{2!}\frac{\partial^2 g}{\partial v^2}(v_e) + \text{h.o.t} \tag{4.13}$$

$$z_{-1} \equiv g(v_e - h) = g(v_e) - h\frac{\partial g}{\partial v}(v_e) + \cdots \tag{4.14}$$

In equation 4.13 and equation 4.14, z_1 and z_{-1} represent forward and backward propopagation. From equation 4.13 and 4.14, it can be easily seen that the equation below is obtained if order h^2 and higher order terms are ignored. h term represents the perturbation amount.

$$\left.\frac{\partial g}{\partial v}\right|_{v=v_e} = \frac{z_1 - z_{-1}}{2h} \tag{4.15}$$

The methodology behind the linearization has been given, now the equations used in the linearization of Remus-100 will be givenin detail. The outputs of the dynamic model used are in equation 4.7 format and show the time-dependent change of the dynamic model states. Using these time-dependent changes, matrices A and B are found as shown below. Forward and backward perturbation will be defined for A matrix as x_1 and x_{-1} according to the point (x_e, u_e).

$$x_1 = f(x_e + h, u_e) \tag{4.16}$$

$$x_{-1} = f(x_e - h, u_e) \tag{4.17}$$

$$A = \frac{\partial f}{\partial x}\Big|_{x=x_e} = \frac{x_1 - x_{-1}}{2h} \tag{4.18}$$

$$h = 0.00001 \tag{4.19}$$

From equation 4.16 , equation 4.17 and equation 4.18, calculation process of A matrix can be seen. x_1 and x_{-1} represent forward and backward perturbation for states AUV and h represents perturbation amount. After obtaining A matrix, B matrix will be found. To find this matrix, forward and backward perturbation will be defined for B matrix as u_1 and u_{-1} according to the point (x_e, u_e).

$$u_1 = f(x_e, u_e + h) \tag{4.20}$$

$$u_{-1} \equiv f(x_e, u_e - h) \tag{4.21}$$

$$B = \frac{\partial f}{\partial u}\Big|_{u=x_e} = \frac{u_1 - u_{-1}}{2h} \tag{4.22}$$

From equation 4.20 , equation 4.21 and equation 4.22, calculation process of A matrix can be seen. It should be noted that A and B matrices were created using the first 12 of the 15 states defined in equation 2.1. Therefore, matrix A was obtained in size 12x12 and matrix B was obtained in size 12x2 since there are 2 control surfaces. Finally, the linearization process ended and the A, B matrices required for the design of the controller were obtained. Additionally, linearization is performed at every step of the simulation. The problem of path following is converted into a regulation problem by

finding deviations of system states that need to be controlled. The obtained LQR control law can be shown in this way as follows simply.

$$u(t) = -K(t)\tilde{x}(t) \tag{4.23}$$

$$\tilde{x}(t) = x(t) - x_{ref}(t) \tag{4.24}$$

In equation 4.23 and equation 4.24, $u(t)$ is the control input vector, $K(t)$ is feedback control gain matrix, $x_{ref}(t)$ represents reference states, $\tilde{x}(t)$ represents state error vector. The feedback control gain matrix is calculated by minimizing the following cost function.

$$J = \int_{t_0}^{t_f} (x^T Q x + u^T R u) dt \tag{4.25}$$

In equation 4.25, t_0, t_f are the initial and final time for the mission respectively. Now the Q and R weighting matrices will be defined as shown below.

$$Q = diag(1, 1, 1, 1, 1, 100, 1, 1, 200, 1, 1, 1000) \tag{4.26}$$

$$R = \begin{vmatrix} 0.1 & 0 \\ 0 & 0.2 \end{vmatrix} \tag{4.27}$$

Finally, the entire process to calculate the coefficients of the LQR controller was mentioned. MATLAB's lqr function was used when calculating the LQR controller gain. The coefficients of the controller were updated at each simulation step. In this context, the depth and heading angle of the AUV were checked. Since the AUV does not have any control surface to control the rolling angle, the rolling angle is controlled, already the Remus -100 AUV is an AUV with natural rolling stability. This process can be seen comprehensively in the figure below.

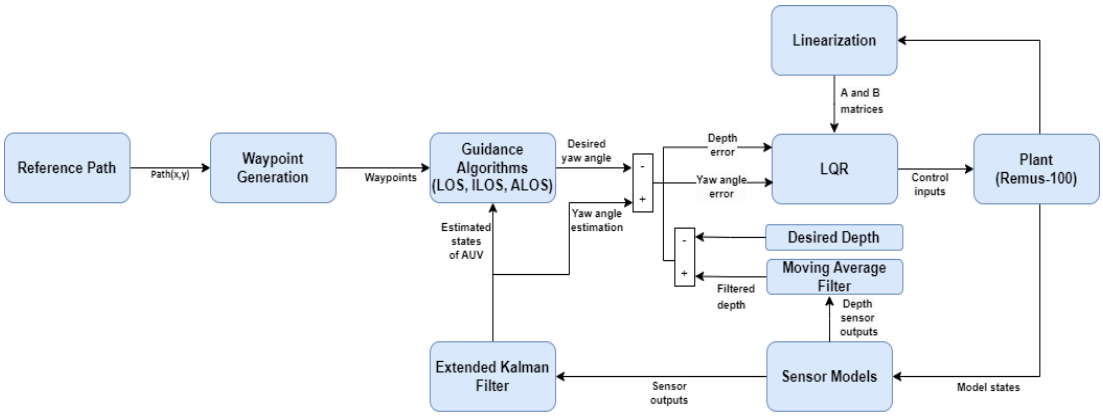

Figure 4.1 : General overview of the control architecture.

The LQR design process has been explained so far, and the performance testing of the controller will be discussed in the next subsection.

4.2 Testing and Results of LQR

This section will focus on the performance of the developed LQR controller. In this context, the yaw angle and how it follows will be examined. First, yaw angle following behavior will be examined. In this context, variable yaw angle command values will be given and LQR's response to these commands will be examined in Figure 4.2.

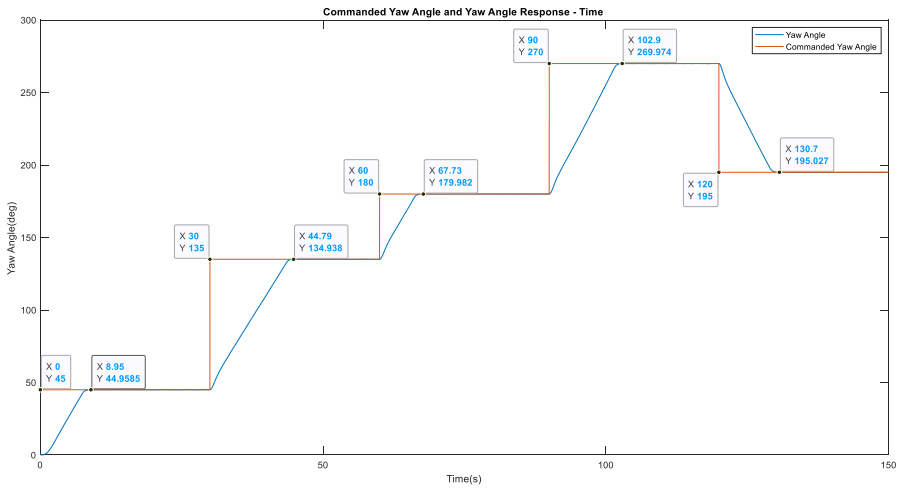

Figure 4.2 : Commanded yaw angle and yaw angle response of LQR.

In Figure 4.2, when the yaw angle commands are examined, it is seen that there are yaw angle commands that change at certain moments. LQR, on the other hand, seems to respond quickly to these commands when considering an underwater system. There is no oscillation movement around the commanded yaw angle value. Also, steady state

error is not seen in the yaw angle response. In Figure 4.3, the use of the control surface while performing these maneuvers will be mentioned.

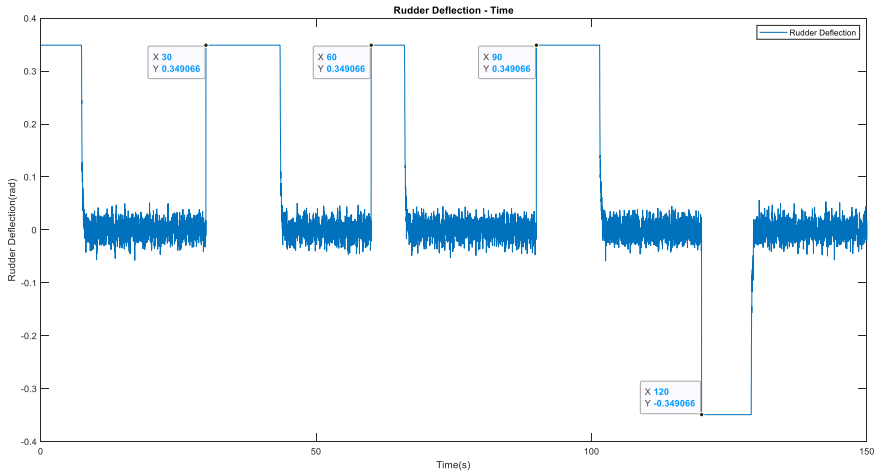

Figure 4.3 : Rudder deflection during these maneuvers.

In Figure 4.3, when the use of rudder control surface is examined, very few control surface is used. As soon as the command came, the full rudder command came and as it approached the commanded yaw angle, the control surface is used with minimum deflection. Based on this information, it can be seen that LQR can control the yaw angle command properly. After examining the LQR's yaw angle response, its response to depth commands will now be examined. In this context, different depth commands will be given at different times and the response of LQR to these commands will be examined. How the AUV fits into the commanded depth profile will be examined. When the Figure 4.4 is examined, the depth command and the depth of the AUV despite this depth command are seen.

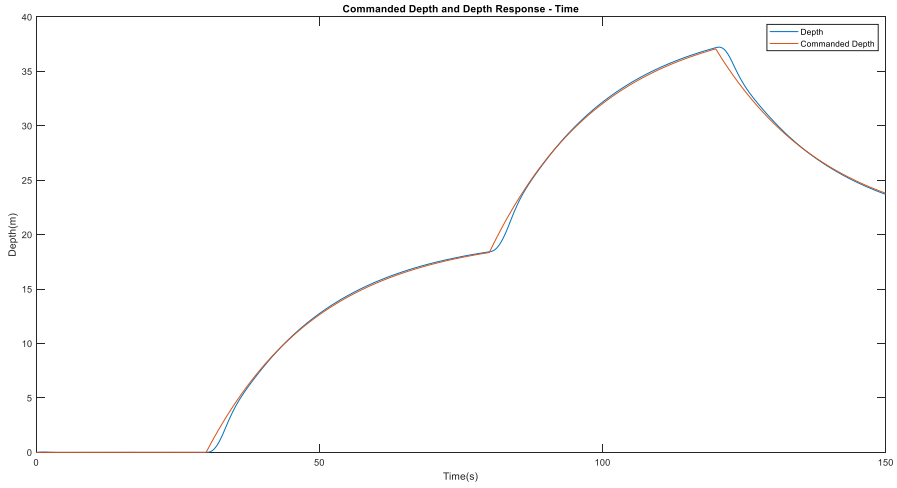

Figure 4.4 : Commanded depth and depth response of LQR.

In Figure 4.4, when the depth commands are examined, it is seen that there are depth commands that change at certain moments. LQR, on the other hand, seems to respond quickly to these commands when considering an underwater system. There is no oscillation movement around the commanded depth value. Also, steady state error is not seen in the depth response. In Figure 4.5, the use of the control surface while performing these maneuvers will be mentioned.

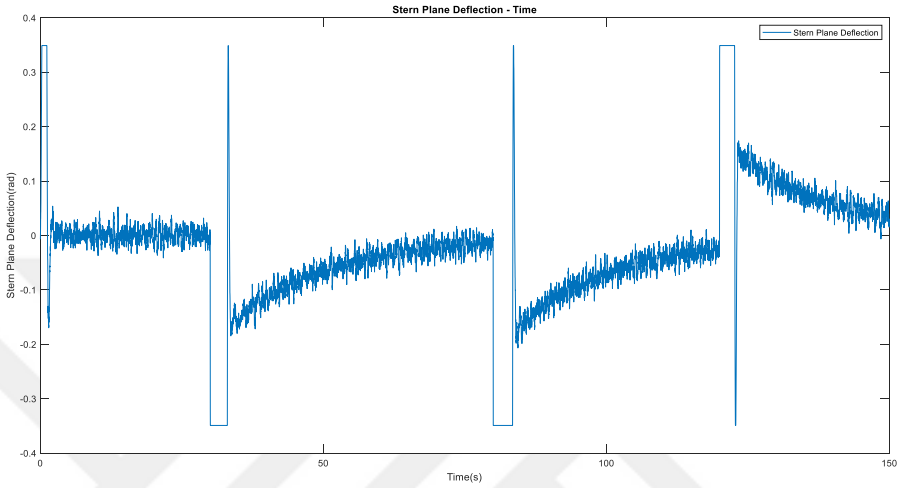

Figure 4.5 : Stern plane deflection during these depth maneuvers.

In Figure 4.5, when the use of stern plane control surface is examined, it is concluded that very few control surface is used. As soon as the command came, the full stern plane command came and as it approached the commanded depth, the control surface is used with less deflection. Based on this information, it can be seen that LQR can control the depth command properly. As a result of these tests, it is concluded that LQR shows sufficient performance to perform the path following mission.

5. DESIGN OF GUIDANCE LAWS FOR PATH FOLLOWING

First, in this chapter, the guidance algorithms designed to perform the path following task will be explained. In this context, LOS, ILOS, ALOS guidance laws were designed to perform the path following task. It should be reminded again that in this study, paths determined on a two-dimensional plane will be followed, that is, there will be movement at a constant depth and only in the xy plane. As output, these guidance laws will calculate which yaw angle should be applied in order for the AUV to instantly follow the desired path.

5.1 Line of Sight Guidance Law

First of all, before explaining the LOS guidance law, it is necessary to explain the terms in the formulation on a visual. In this context, representation of the path following for 2-D with LOS guidance for autonomous marine vehicle (AMV) is shown as follows in Figure 5.1.

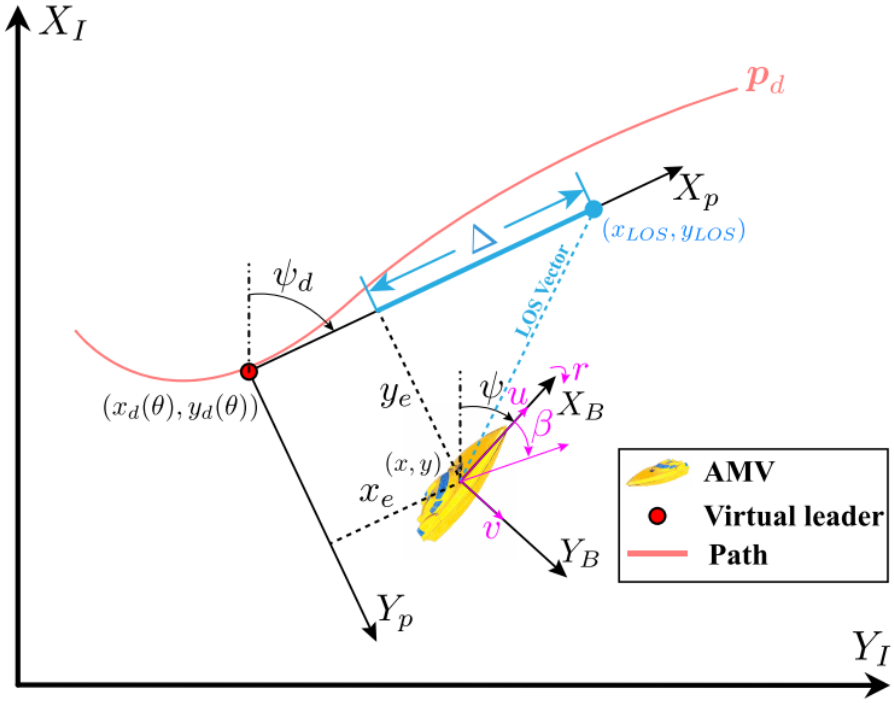

Figure 5.1 : LOS guidance for 2-D path following of an AMV [42].

In Figure 5.1, X_I, Y_I represent inertial reference frame coordinates, X_P, Y_P represent tangential reference frame coordinates defined on the path, X_B, Y_B represent body reference frame coordinates, x_e, y_e represent path following errors, $x_d(\theta)$, $y_d(\theta)$ represent virtual leader waypoint position, virtual leader means active waypoint in guidance terminology. Ψ_d, Ψ represent path tangential angle and actual yaw angle of vehicle respectively. Δ represents lookahead distance, u, v, r represent body velocity components and yaw rate component respectively. Finaly, β represents sideslip angle. So far, the notation used in LOS and its variants, ILOS and ALOS, has been mentioned. Now, the LOS guidance law formulation will be discussed as follows[42].

$$\Psi_c = \Psi_d(\theta) - arctan\left(k_p^{\psi}.y_e\right) - \beta \tag{5.1}$$

$$\Psi_d(\theta) = atan2(y_d^{\theta}, x_d^{\theta}) \tag{5.2}$$

$$x_d^{\theta} = \frac{\partial x_d(\theta)}{\partial \theta} \tag{5.3}$$

$$y_d^{\theta} = \frac{\partial y_d(\theta)}{\partial \theta} \tag{5.4}$$

$$\mathrm{k_p^{\psi}} = \frac{1}{\Delta_{\Psi}} \tag{5.5}$$

$$\beta = atan2(v, u) \tag{5.6}$$

$$y_e = -\left(x - x_d(\theta)\right)\sin\left(\Psi_d(\theta)\right) + (y - y_d(\theta))\cos(\Psi_d(\theta)) \tag{5.7}$$

$$\Delta_{\Psi} = 10\ m \tag{5.8}$$

In equation 5.1, formulation of commanded yaw angle is given, Ψ_c represents commanded yaw angle, $\Psi_d(\theta)$ represents path tangential angle, $arctan(.)$ represents inverse tangent function, k_p^{ψ} is positive proportional gain, y_e is cross track error. Finally, β is sideslip angle. In equation 5.2, formulation of path tangential angle is given and $y_d^{\theta}, x_d^{\theta}$ are partial derivatives according to θ. $atan2(.)$ is a four-quadrant inverse tangent function. In equation 5.3 and equation 5.4, calculations of partial derivatives according to θ are given. In equation 5.5, formula of positive proportional is given and Δ_{Ψ} is positive lookahead distance parameter. In equation 5.6, sideslip

angle calculation is given, u, v are body velocity component with respect to x and y axis respectively. In equation 5.7, formulation of cross track error is given, x, y are the position components of AUV in inertial frame. Finally, positive lookahead distance parameter is selected as 10 meter as shown in equation 5.8.

The entire formulation of the LOS guidance law is given with the equations given so far. The guidance law will be tested with a test scenario. In this context, a circular path has been defined and path following results are shown below in Figure 5.2. In addition cross track error during this test is shown in Figure 5.3.

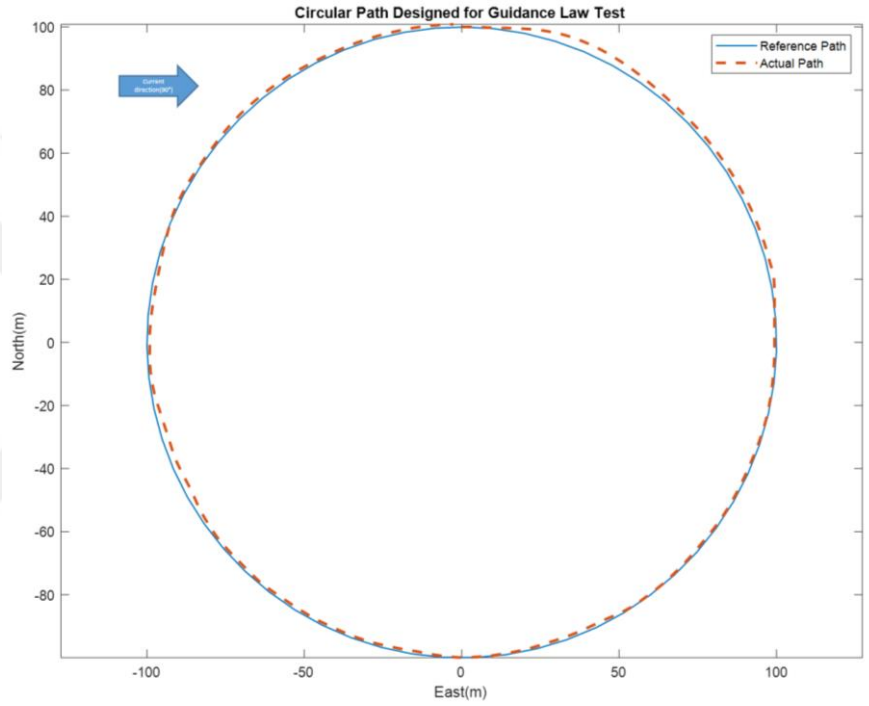

Figure 5.2 : Circular path scenario for LOS guidance.

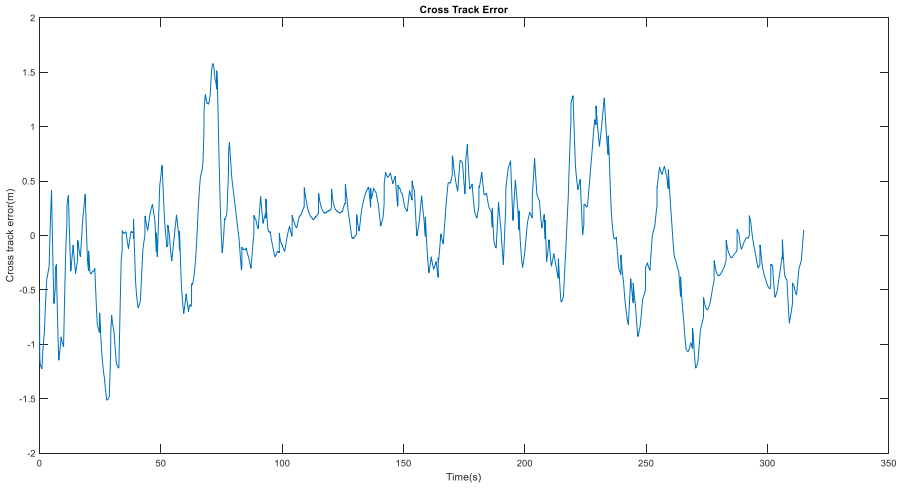

Figure 5.3 : Cross track error for the circular path scenario.

In Figure 5.2, the desired path and actual path of AUV can be seen. In addition, the starting point of the AUV for this test is (100, 0) m. It should be noted that in this scenario, current disturbance was added to the environment, the characteristics of this disturbance are as follows. As seen in Figure 5.2, current direction is 90° and current magnitude is 0.4 m/s. Despite the current disturbance, appropriate yaw angle commands were generated to follow the path defined through the LOS guidance law, so the AUV was able to follow the defined path with low errors. In this context, the cross track error was chosen as the error parameter during the evaluation phase of the guidance law. The cross track error resulting from the test can be seen in Figure 5.3. When this error parameter was evaluated, a maximum cross track error of 1.5 m emerged. In addition, when looking at the overall trend, the cross track error generally appeared below 0.5 meters. Second path for the test is sinusoidal path as shown in Figure 5.4.

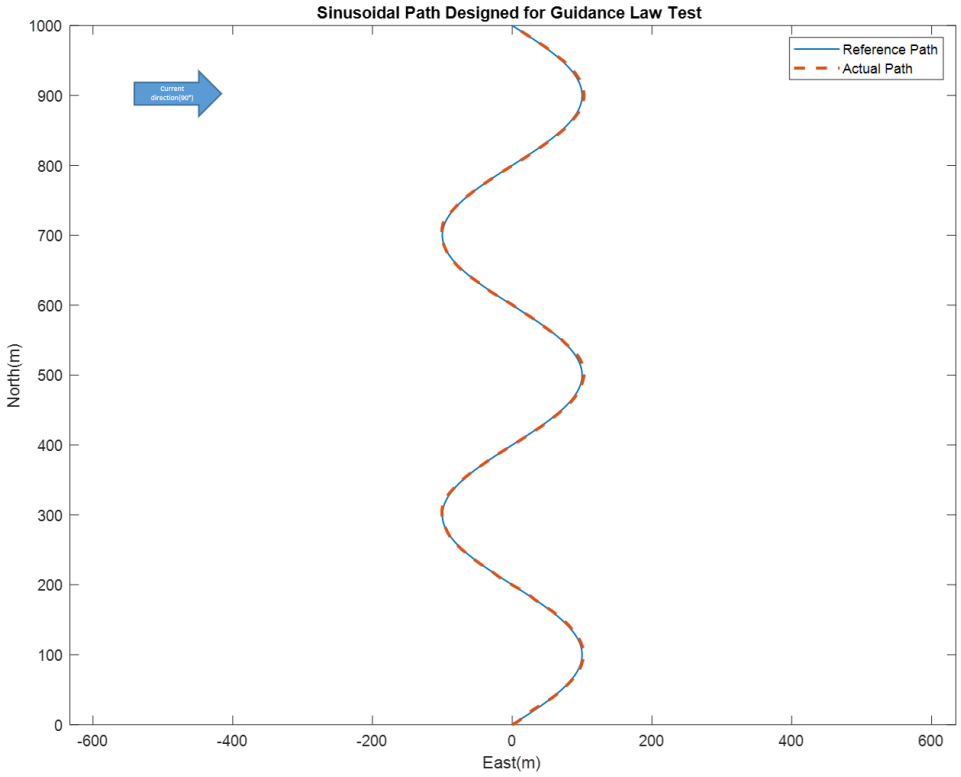

Figure 5.4 : Sinusoidal path scenario for LOS guidance.

When tested with a sinusoidal path, it can be clearly seen in Figure 5.4 that the AUV was able to follow the defined path despite being exposed to current disturbance. In addition, the starting point of the AUV for this test is (0, 0) m. It should be noted that throughout this test, the AUV was commanded to operate 2 m/s and the current

disturbance velocity was 0.4 m/s. In order to make a more detailed analysis, the cross track error parameter given in Figure 5.5 will be examined.

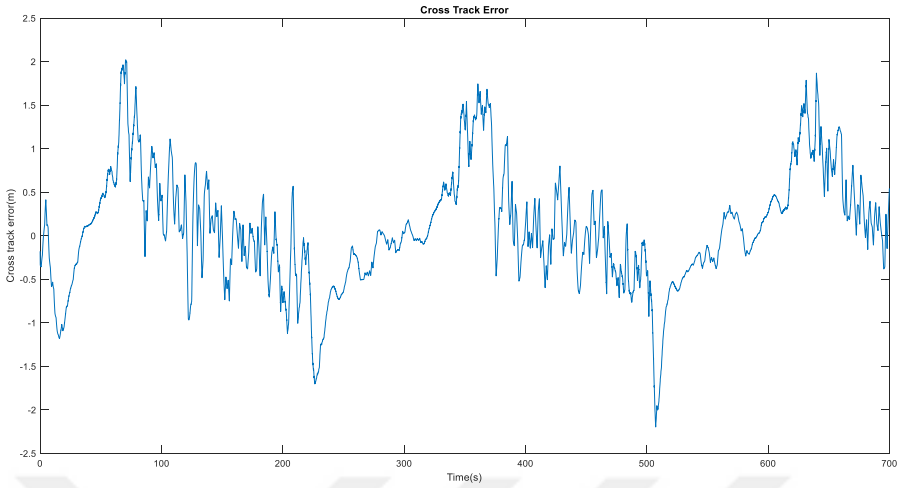

Figure 5.5 : Cross track error for the sinusoidal scenario.

When this error parameter is evaluated, a maximum cross track error of 2 m emerged. In addition, when looking at the overall trend, the cross track error generally appeared below 0.5 meters. As a result, it is concluded that the path following task with LOS guidance has been completed successfully.

5.2 Integral Line of Sight Guidance Law

Now, the ILOS guidance law formulation will be mentioned. This guidance law is a variant of the LOS guidance law and can be considered as a version created by adding the integral term. The relevant equations are mentioned below [42].

$$\Psi_c = \Psi_d(\theta) - arctan\left(k_p^{\psi}.y_e + k_{int}^{\psi}.y_{int}\right) \tag{5.9}$$

$$\dot{y}_{int} = \frac{\Delta_{\psi}.y_e}{{\Delta_{\psi}}^2 + (y_e + k_{int}^{\psi}.\Delta_{\psi}.y_{int})^2} \tag{5.10}$$

$$y_{int_0} = 0 \tag{5.11}$$

$$k_p^{\psi} = \frac{1}{\Delta_{\psi}} \tag{5.12}$$

$$\Delta_{\psi} = 10\ m \tag{5.13}$$

$$k_{int}^{\psi} = 0.18 \tag{5.14}$$

In equation 5.9, formulation of commanded yaw angle for ILOS guidance law is given. Ψ_c represents commanded yaw angle, $\Psi_d(\theta)$ represents path tangential angle. $arctan(.)$ represents inverse tangent function, $k_p^{\psi}, k_{int}^{\psi}$ are positive proportional gain and positive integral gain respectively. y_e is cross track error, y_{int} is the integral term. This integral term is calculated by using equation 5.10. Δ_{ψ} is positive lookahead distance parameter in this equation. In equation 5.11, y_{int_0} is initial value of integral term. Finally, the entire formulation of the ILOS guidance law is given with the equations given so far. The guidance law will be tested with a test scenario. In this context, a circular path has been defined and path following results are shown below in Figure 5.6. In addition cross track error during this test is shown in Figure 5.7.

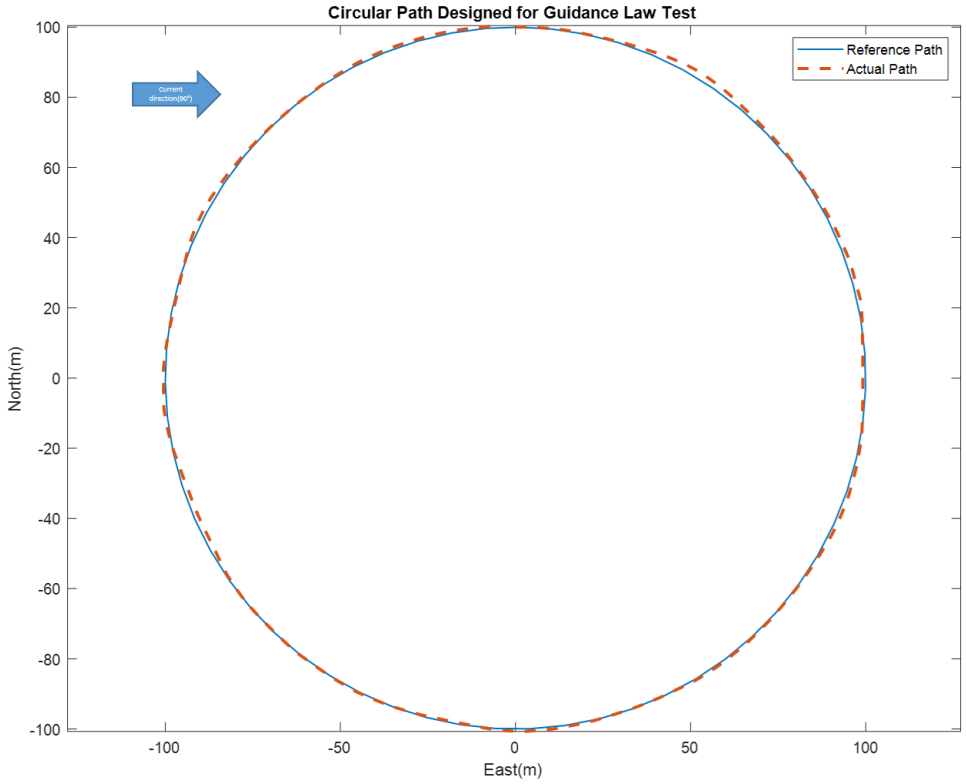

Figure 5.6 : Circular path scenario for ILOS guidance.

In Figure 5.6, the desired path and actual path of AUV can be seen. In addition, the starting point of the AUV for this test is (100, 0) m. Current disturbance exists in this test, the characteristics of this disturbance are as follows. Current direction is 90° and current magnitude is 0.4 m/s. Despite the current disturbance, the defined path was followed by AUV through the ILOS guidance law, so the AUV was able to follow the

defined path with low track errors. Now, the cross track error will be examined as the error parameter during the evaluation phase of the guidance law. The cross track error resulting from the test can be seen in Figure 5.7. When this error parameter was evaluated, a maximum cross track error of 1.4 m emerged. In addition, when looking at the overall trend, the cross track error generally appeared below 0.5 meters.

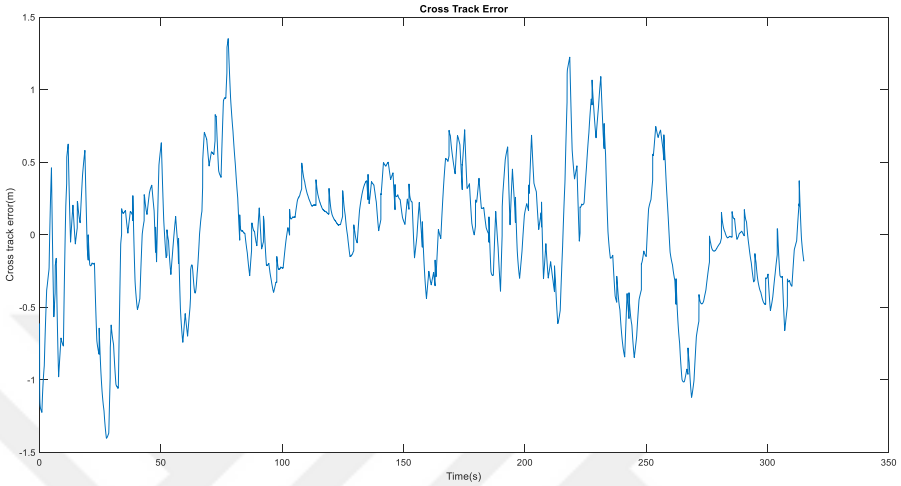

Figure 5.7 : Cross track error for the circular path scenario.

Second path for the test is sinusoidal path as shown in Figure 5.8. In addition, the starting point of the AUV for this test is (0, 0) m. When the figure is examined, in this test, the AUV was exposed to current disturbance as in the circular path, but it can be seen that the AUV can follow the defined path.

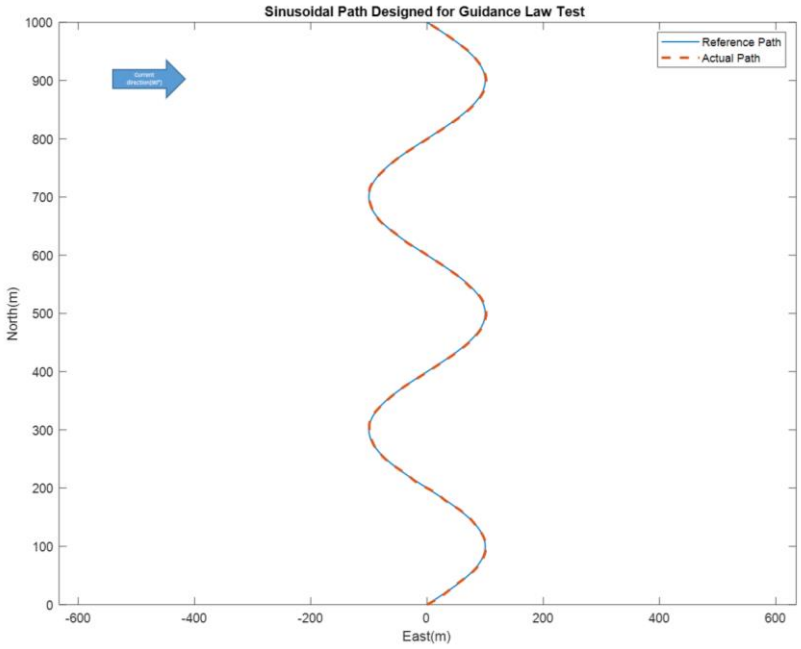

Figure 5.8 : Sinusoidal path scenario for ILOS guidance.

Finally, when the cross track error parameter is examined in Figure 5.9, it is seen that a maximum error of -1.6 m is observed and mostly this error is below 0.5 m. As a result, it is concluded that the path following task with ILOS guidance has been completed successfully.

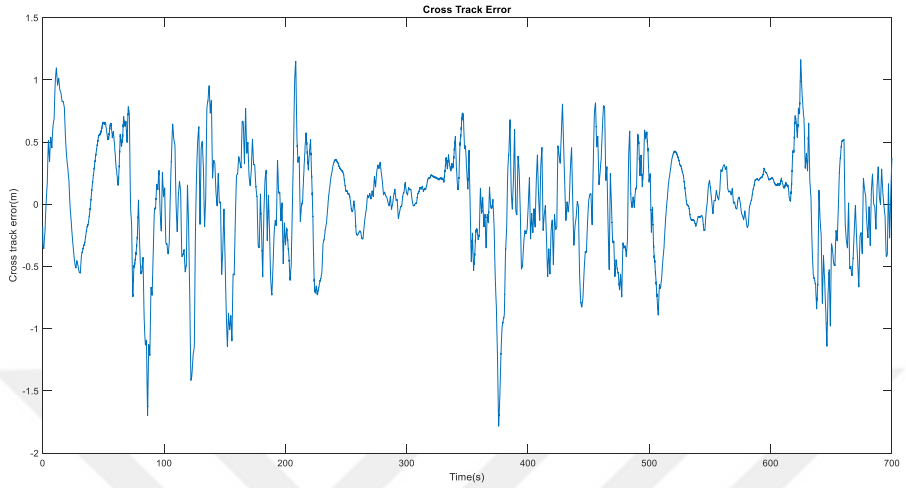

Figure 5.9 : Cross track error for the sinusoidal path scenario.

5.3 Adaptive Line of Sight Guidance Law

Now, the ALOS guidance law formulation will be mentioned. This guidance law is a variant of the LOS guidance law. This guidance law can be considered as a variant of LOS guidance, which is created by estimating crab angle component. Therefore, the formulation behind the ALOS is very similar to formulation of LOS guidance. The relevant equations are mentioned below [33].

$$\Psi_c = \Psi_d(\theta) - \hat{\beta}_c - arctan\left(\frac{y_e}{\Delta_\Psi}\right) \tag{5.15}$$

$$\dot{\hat{\beta}}_c = \frac{\gamma . \Delta_\Psi . y_e}{\sqrt{{\Delta_\Psi}^2 + {y_e}^2}} \tag{5.16}$$

$$\hat{\beta}_{c_0} = 0 \tag{5.17}$$

$$\Delta_\Psi = 10\ m \tag{5.18}$$

$$\gamma = 0.012 \tag{5.19}$$

In equation 5.15, formulation of commanded yaw angle for ALOS guidance law is given. Ψ_c represents commanded yaw angle, $\Psi_d(\theta)$ represents path tangential angle, $\hat{\beta}_c$ is crab angle estimate, $arctan(.)$ represents inverse tangent function. y_e is cross track error, Δ_ψ is positive lookahead distance parameter in this equation. In equation 5.16, the formulation of time derivative of crab angle estimate is given. γ is adaptation gain. In equation 5.17, initial value of crab angle estimate is given. Finally, in equation 5.18 and equation 5.19, values of positive lookahead distance and adaptation gain can be seen. The ALOS guidance law will be tested in the same manner as the LOS and ILOS guidance laws. In this context, one circular and one sinusoidal path will be defined and the AUV will be able to follow these paths with the help of ALOS. In this context, a circular path has been defined and path following results are shown below in Figure 5.10. In addition cross track error during this test is shown in Figure 5.11.

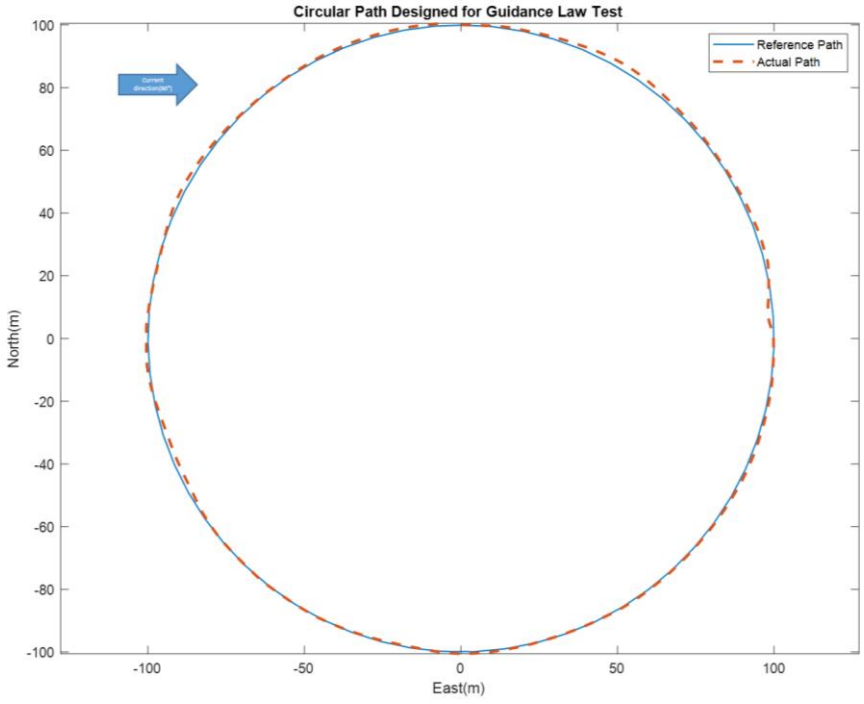

Figure 5.10 : Circular path scenario for ALOS guidance.

In Figure 5.10, the desired path and actual path of AUV can be seen. In addition, the starting point of the AUV for this test is (100, 0) m. Current disturbance exists in this test, the characteristics of this disturbance are same as other tests. Despite the current disturbance, the defined path was followed by AUV through the ALOS guidance law, so the AUV was able to follow the defined path with low track errors. Now, the cross track error will be examined as the error parameter during the evaluation phase of the guidance law. The cross track error resulting from the test can be seen in Figure 5.11.

When this error parameter was evaluated, a maximum cross track error of 1.5 m emerged. In addition, when looking at the overall trend, the cross track error generally appeared below 0.5 meters.

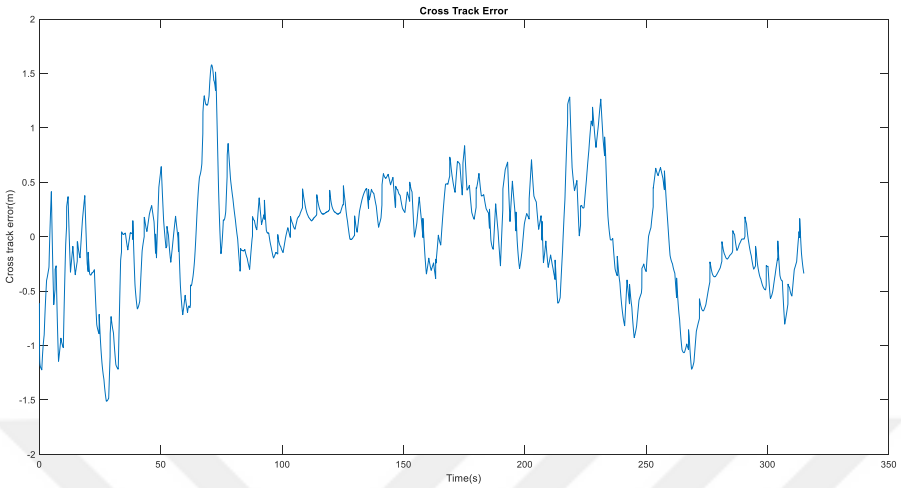

Figure 5.11 : Cross track error for the circular path scenario.

Second path for the test is sinusoidal path as shown in Figure 5.12. In addition, the starting point of the AUV for this test is (0, 0) m. When the figure is examined, in this test, the AUV was exposed to current disturbance as in the circular path, but it can be seen that the AUV can follow the defined path.

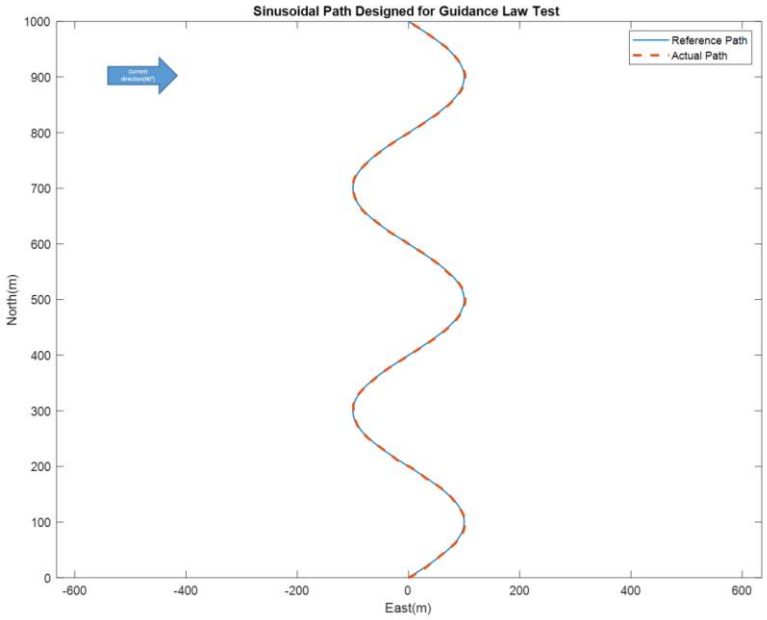

Figure 5.12 : Sinusoidal path scenario for ALOS guidance.

Finally, when the cross track error parameter is examined in Figure 5.13, it is seen that a maximum error of -1.9 m is observed and mostly this error is below 0.5 m. As a

result, it is concluded that the path following task with ALOS guidance has been completed successfully.

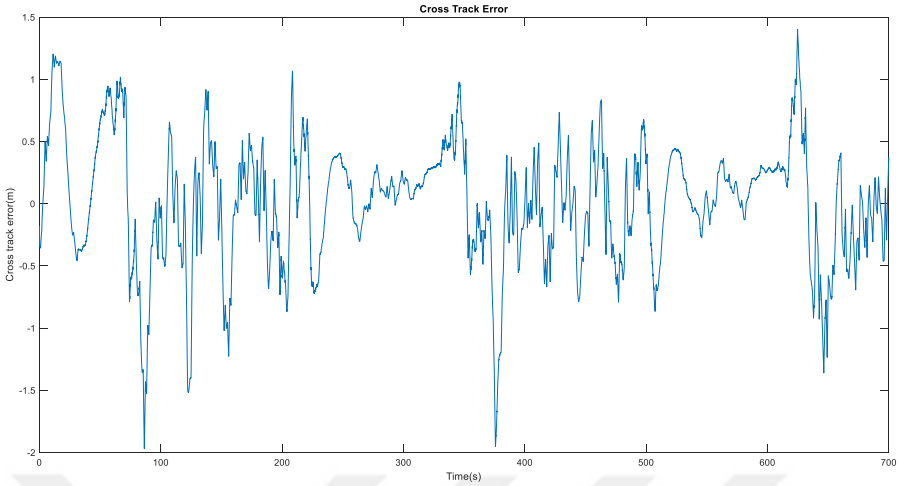

Figure 5.13 : Cross track error for the sinusoidal path scenario.

As a result, 3 different guidance law designs used in this study have been described so far. Afterwards, they were tested on two paths to observe the performance of each guidance law. The results obtained were satisfactory. Finally, it should be noted that the main purpose of this study is to evaluate the performance of these three guidance techniques by defining different paths and exposing them to different current disturbance conditions. The next chapter will focus on these issues.

6. TEST AND RESULTS

First of all, all the sub-components defined so far to perform the path following task have been mentioned. If they are briefly mentioned again, the first thing to do is to develop EKF to be able to perform the state estimation task and to test the developed algorithm under more realistic conditions because operational AUVs also approach the problem in this way. In addition, the AUV must be controllable in order to perform the path following task, and in this context, a controller was developed with the LQR method. Finally, the main focus of this study was the development of guidance laws and their performance comparison. The guidance laws developed in this process are LOS, ILOS, and ALOS guidance laws. All these mentioned controller, navigation and guidance sub-components were tested separately during the design process. In this chapter, the final algorithm will be tested when all the sub-components are together.

6.1 Test Scenarios

While testing the performance of the algorithms developed in this subchapter, the conditions under which they were tested will be mentioned. In this context, the tests of 3 different guidance algorithms that have already been developed were carried out as follows. 4 different paths were defined. The circular path defined in Figure 6.1 can be seen.

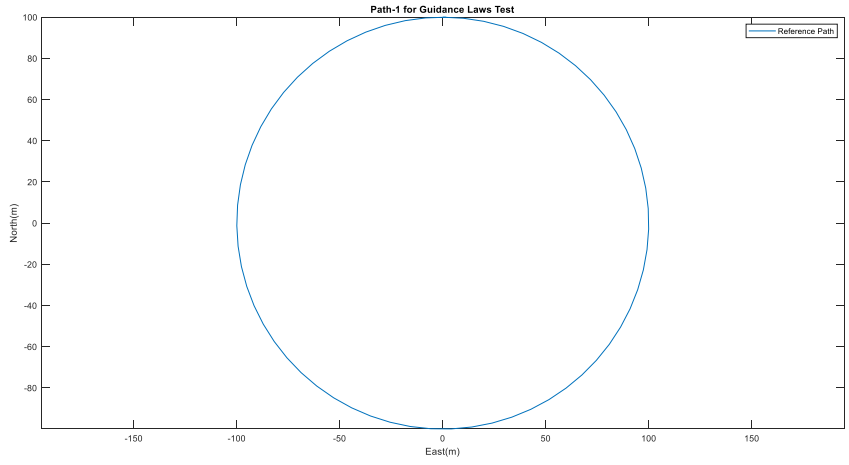

Figure 6.1 : Path-1 for guidance laws test.

These paths were classified as follows: Path-1 is a circular path, Path-2 is a straight path, Path-3 is a semi-rectangular path, and Path-4 is a sinusoidal path. Path-2 can be seen in Figure 6.2.

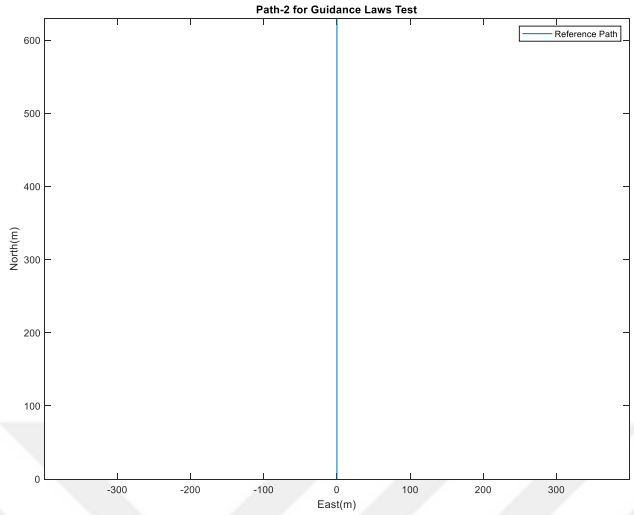

Figure 6.2 : Path-2 for guidance laws test.

Semi-rectangular path being path-3 can be seen in Figure 6.3.

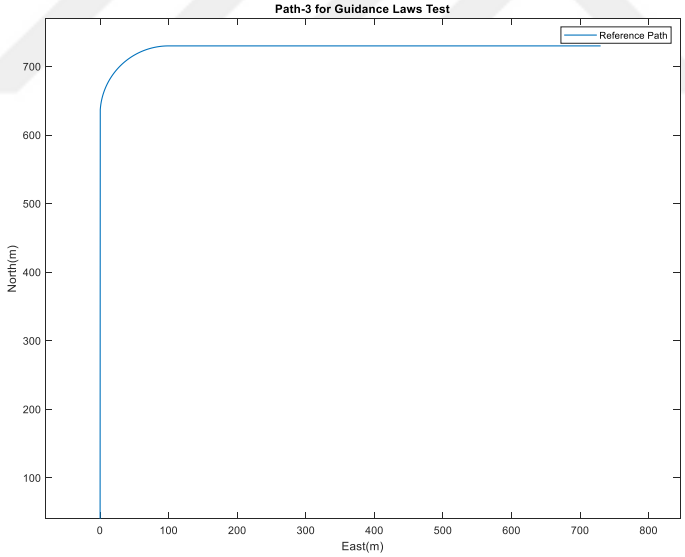

Figure 6.3 : Path-3 for guidance laws test.

In addition, disturbance was added to the environment because the AUV may be exposed to environmental disturbance while operating on these paths, and this disturbance is current disturbance. This disturbance component is already among the inputs of the dynamic model of Remus-100 AUV. In order to test the performance of the guidance laws, it was planned to be exposed to current disturbance in different

directions and at different velocities and they were tested in this way. Finally, sinusoidal path being path-4 can be seen in Figure 6.4.

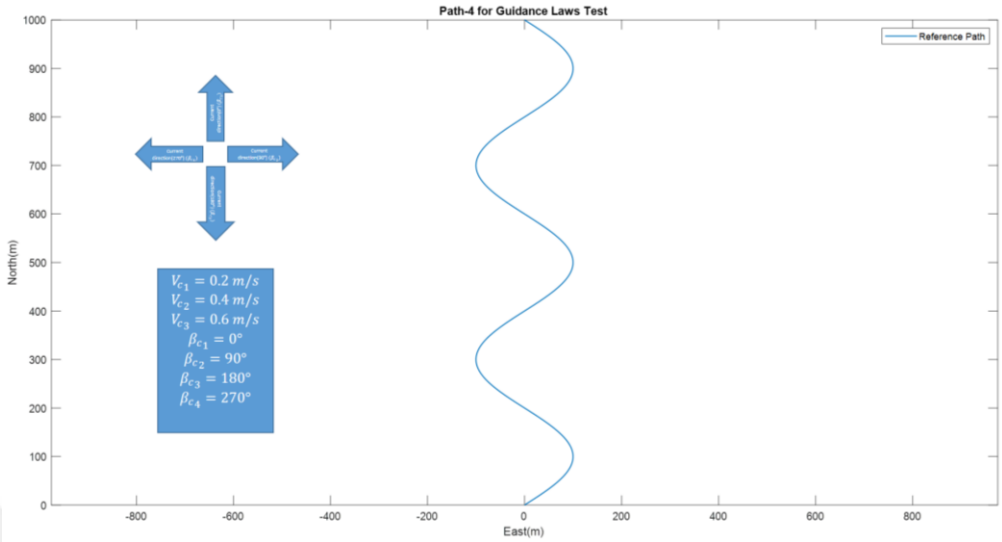

Figure 6.4 : Path-4 for guidance laws test.

In Figure 6.4, there are representations of current velocities and current directions that were mentioned earlier. $V_{c_1}, V_{c_2}, V_{c_3}$ are current velocity components. $\beta_{c_1}, \beta_{c_2}, \beta_{c_3}$ and β_{c_4} are current direction components.

6.2 Test Results

Test scenarios have been mentioned so far, it will examine how the AUV follows 4 different paths with 3 different guidance laws, 3 different current velocities, and 4 different current directions. This means that 144 simulations will be run in the tests and the results will be evaluated. The most important evaluation criterion in this context is the cross-track error component, as mentioned in the earlier chapter. Because this component is the perpendicular distance to the line drawn on the tangent of the instantly active waypoint, which is the lateral distance to the path that the AUV should follow on straight paths, therefore, this parameter is an important evaluation criterion. The fact that it is currently one of the main parameters in the formulations of all guidance laws proves this. The formulation of this parameter is given in equation 6.1 below.

$$y_e = -\big(x - x_d(\theta)\big)\sin\big(\Psi_d(\theta)\big) + (y - y_d(\theta))\cos(\Psi_d(\theta)) \tag{6.1}$$

In equation 6.1, x, y represent position of AUV, $x_d(\theta), y_d(\theta)$ are the position of active waypoint. $\Psi_d(\theta)$ is path tangential angle. Finally, y_e is the cross track error. After the cross track error is defined, the results will now be mentioned. The mean and standard deviations of cross track error are given in the tables as results. Using these results, the performances of the guidance laws will be compared. The reason for using cross track error for performance comparison can be explained as follows. When the purpose of the path following task is examined, the most important criterion of performance is related to how far the AUV is laterally from the defined path, and the cross track error component is a component related to this phenomenon. First, when taking a general look at the tables, the general structure of the tables is as follows. First of all, each table consists of data calculated for a current direction value and for 3 different current velocity components. In this context, the mean and standard deviations of the cross track error data obtained throughout the entire tests are calculated in the tables, and the unit of these calculated values is meters. Table 6.1 and Table 6.2 contain the results for current direction 1 ($\beta_{c_1} = 0°$) as shown below.

Table 6.1 : Mean(m) of cross track error for $\beta_{c_1} = 0°$.

	V_{c_1}			V_{c_2}			V_{c_3}		
Path	LOS	ILOS	ALOS	LOS	ILOS	ALOS	LOS	ILOS	ALOS
1	0.8507	0.4790	0.4928	0.8273	0.4951	0.5478	0.8750	0.7400	0.9738
2	0.7096	0.7256	0.9798	0.6897	0.8327	0.9977	0.7160	0.6689	0.7386
3	0.5018	0.7077	0.7136	0.5144	0.6626	0.6923	0.5231	0.5814	0.6027
4	0.5820	0.4358	0.4878	0.6375	0.5407	0.6193	0.7296	1.0309	0.8162

Table 6.2 : Standard deviation(m) of cross track error for $\beta_{c_1} = 0°$.

	V_{c_1}			V_{c_2}			V_{c_3}		
Path	LOS	ILOS	ALOS	LOS	ILOS	ALOS	LOS	ILOS	ALOS
1	0.9942	0.6466	0.6967	0.9791	0.6779	0.7676	1.0298	1.0196	1.3774
2	0.9144	0.8591	1.1534	0.9054	0.9710	1.1492	0.9301	0.8223	0.9095
3	0.6742	0.9371	0.9067	0.6910	0.7654	0.8662	0.7080	0.7245	0.7598
4	0.8003	0.6056	0.6847	0.8924	0.7468	0.8359	1.0649	1.0500	1.1350

When Table 6.1 and Table 6.2 are examined, the test results of the simulations where the AUV is exposed to current disturbance on the 0° route are seen. It can be seen that the AUV had the best performance with the ILOS guidance law while following the circular path-1, and also the ALOS guidance law has performed so well. This result can be understood from the values of the cross-track error mean and standard

deviation. Briefly, if the performances are ranked from best to worst, they can be expressed as ILOS>ALOS>LOS. When the test results of path-2, which is a straight path, are compared, it is seen that LOS guidance works at higher performance than ILOS and ALOS guidance laws. This is evident because the mean and standard deviation values are lower for LOS guidance. Additionally, when the values in Table 6.1 and Table 6.2 are examined, the second best guidance law in following path-2 is ILOS guidance law. As a result, when sorting from best performance to worst performance in tracking path-2, the following conclusion is reached, LOS>ILOS>ALOS. Now, the semi-rectangular path-3 will be examined. In this context, when the data in Table 6.1 and Table 6.2 are examined, the following conclusion is reached, LOS guidance has shown better performance than the other two methods, and ILOS follows LOS in terms of performance. As the speed of current disturbances increases, the average cross-track error naturally increases. This is an expected fact, the AUV is currently traveling at a speed of 2 m/s, and when the current speed component becomes 0.6 m/s, that is, 30% of its speed, a decrease in the performance of the AUV is expected. Briefly, as a result of comparing the performances of AUVs for path-3, when their performances are compared from best to worst, the following conclusion is reached, LOS>ILOS>ALOS. Comparing the performance results for path-4, which has a sinusoidal profile, the following conclusions are reached: ILOS guidance law showed the best performance because the cross-track error mean and standard deviation had the lowest value with ILOS guidance. In Tables 6.1 and 6.2 when the values are examined, ALOS guidance law has the second-best performance. As a result, when their performances were ranked from best to worst, the following conclusion was reached, ILOS>ALOS>LOS.

Secondly, Table 6.3 and Table 6.4 contain the results for current direction 2 ($\beta_{c_2} = 90°$) as shown below.

Table 6.3 : Mean(m) of cross track error for $\beta_{c_2} = 90°$.

	V_{c_1}			V_{c_2}			V_{c_3}		
Path	LOS	ILOS	ALOS	LOS	ILOS	ALOS	LOS	ILOS	ALOS
1	0.9282	0.4462	0.5090	0.9257	0.5002	0.5338	0.9737	0.5184	0.5798
2	0.5123	0.4979	0.5311	0.4655	0.5010	0.5487	0.4589	0.5513	0.6024
3	0.4744	0.4759	0.5241	0.4849	0.4912	0.5504	0.5045	0.5221	0.5998
4	0.5637	0.4084	0.4387	0.5829	0.4826	0.5263	0.5896	0.5529	0.5950

Table 6.4 : Standard deviation(m) of cross track error for $\beta_{c_2} = 90°$.

	V_{c_1}			V_{c_2}			V_{c_3}		
Path	LOS	ILOS	ALOS	LOS	ILOS	ALOS	LOS	ILOS	ALOS
1	1.0990	0.5865	0.6570	1.0271	0.6460	0.6833	1.0632	0.6604	0.7157
2	0.6609	0.6292	0.6876	0.5911	0.6320	0.6931	0.5888	0.7154	0.7973
3	0.5975	0.6040	0.6603	0.6152	0.6085	0.6765	0.6649	0.6657	0.7637
4	0.7311	0.5724	0.6192	0.7694	0.6237	0.6807	0.7611	0.7039	0.7644

When the data in Table 6.3 and Table 6.4 are examined, the characteristics of the outputs are quite similar to the outputs where the current direction is 0°. When Path-1 performance outputs were examined, the best performance was again seen in the ILOS guidance law technique. ALOS guidance law follows ILOS guidance law in terms of performance. As a result, when the ranking of the performances is examined, they are listed from best performance to worst performance as follows, ILOS>ALOS>LOS. Likewise, when the path following performances for path-2 are compared, it is seen that when ranked from best to worst, it is LOS>ILOS>ALOS. When the outputs in the table in Path-3 are evaluated, the following conclusion can be drawn, they can be listed from best to worst as LOS>ILOS>ALOS. Finally, when the path-4 outputs are examined, it is seen that it shows similar phenomena as the condition where the current direction is 0°, which can be expressed in the order ILOS>ALOS>LOS. Table 6.5 and Table 6.6 contain the results for current direction 3 ($\beta_{c_3} = 180°$) as shown below.

Table 6.5 : Mean(m) of cross track error for $\beta_{c_3} = 180°$.

	V_{c_1}			V_{c_2}			V_{c_3}		
Path	LOS	ILOS	ALOS	LOS	ILOS	ALOS	LOS	ILOS	ALOS
1	0.8141	0.5187	0.5398	0.8182	0.5653	0.5863	0.8030	0.6221	0.6782
2	0.7182	0.6630	1.0375	0.5986	0.6491	1.0443	0.6120	0.6853	1.0727
3	0.5378	0.5975	0.7697	0.4961	0.5648	0.8427	0.5141	0.6035	0.8171
4	0.5240	0.4334	0.4668	0.5825	0.4867	0.5281	0.6882	0.5413	0.6063

Table 6.6 : Standard deviation(m) of cross track error for $\beta_{c_3} = 180°$.

	V_{c_1}			V_{c_2}			V_{c_3}		
Path	LOS	ILOS	ALOS	LOS	ILOS	ALOS	LOS	ILOS	ALOS
1	0.9501	0.6498	0.6902	0.9496	0.7223	0.7598	0.9320	0.8347	0.9092
2	0.8984	0.7862	1.2371	0.8110	0.8135	1.2084	0.7819	0.8284	1.2462
3	0.6977	0.7352	0.9809	0.6616	0.7094	1.0314	0.6567	0.7443	1.0138
4	0.7060	0.5934	0.6476	0.6322	0.6677	0.7327	0.6487	0.7333	0.8260

Now, when the data in Tables 6.5 and 6.6 are examined, the characteristics of the outputs are quite similar to the outputs where the current direction is 0°. When Path-1 performance outputs were examined, the best performance was again seen in the ILOS guidance law technique. As a result, when the ranking of the performances is examined, they are listed from best performance to worst performance as follows, ILOS>ALOS>LOS. Likewise, when the path following performances for path-2 are compared, it is seen that when ranked from best to worst, it is LOS>ILOS>ALOS. When the outputs in the table in Path-3 are evaluated, the following conclusion can be drawn, they can be listed from best to worst as LOS>ILOS>ALOS. Finally, when the path-4 outputs are examined, it is seen that it shows similar phenomena as the condition where the current direction is 0°, which can be expressed in the order ILOS>ALOS>LOS. Finally, Table 6.7 and Table 6.8 contain the results for current direction 4 ($\beta_{c_4} = 270°$) as shown below.

Table 6.7 : Mean(m) of cross track error for $\beta_{c_4} = 270°$.

	V_{c_1}			V_{c_2}			V_{c_3}		
Path	LOS	ILOS	ALOS	LOS	ILOS	ALOS	LOS	ILOS	ALOS
1	0.8374	0.4979	0.5028	0.8653	0.5347	0.5281	0.8053	0.5365	0.5808
2	0.4531	0.5568	0.5328	0.5028	0.5854	0.6618	0.5143	0.6657	0.7423
3	0.4246	0.5105	0.4863	0.4435	0.5337	0.5608	0.4457	0.5795	0.6162
4	0.5633	0.3818	0.4276	0.5486	0.4037	0.4376	0.52989	0.4169	0.4489

Table 6.8 : Standard deviation(m) of cross track error for $\beta_{c_4} = 270°$.

	V_{c_1}			V_{c_2}			V_{c_3}		
Path	LOS	ILOS	ALOS	LOS	ILOS	ALOS	LOS	ILOS	ALOS
1	0.9975	0.6320	0.6572	1.1326	0.6674	0.6654	1.0514	0.6547	0.6960
2	0.5782	0.6813	0.6618	0.6547	0.7457	0.8277	0.6566	0.8767	0.9807
3	0.5289	0.6486	0.6142	0.5650	0.6838	0.7146	0.5654	0.7576	0.8130
4	0.7706	0.5406	0.6048	0.7609	0.5631	0.6090	0.7374	0.5722	0.6132

Now, when the data in Tables 6.7 and 6.8, which contain the outputs for the last current direction, are examined, they are quite similar to the outputs for the other 3 current directions mentioned so far. In this context, the results obtained as a result of the simulations made in all current directions and current velocities show similar phenomena. Finally, when all tests are examined, the performances for path-1, which is a straight path, are listed from best to worst as ILOS>ALOS>LOS. When comparing the performances for path-2 and path-3, the order from best to worst is

LOS>ILOS>ALOS. Finally, when path-4 is ranked from best to worst, it is ILOS>ALOS>LOS. In addition, as the current velocity disturbance increases, the mean and standard deviation values increase in all outputs, which is expected. Finally, ILOS guidance law, which showed superior performance in path-1 and path-4, showed superior performance in circular and sinusoidal paths, which shows that ILOS guidance gives better results in paths containing curvature. It has been observed that LOS guidance law, which has superior performance in path-2 and path-3, gives good results on flat and rectangular paths, which shows that LOS guidance gives better results on flat paths compared to other methods. In this case, it can be concluded that since the defined paths are predetermined paths, if there are straight lines in the planned path, LOS guidance can be active at that time, and ILOS guidance can be active in the parts of the path that contain curvature, that is, in places where there are turns and maneuvers. This ultimately enables maximum path-following performance to be achieved in all designed paths. Since one guidance law performs better than the other according to the path features, automatic guidance law switching can be performed in AUV tasks by establishing a simple switch-case logic and achieving minimum cross-track error.

7. CONCLUSION

First of all, in this chapter, the final algorithm will be tested when all the sub-components are together. In this chapter, what has been done so far in this study will be briefly mentioned and then the results obtained will be briefly discussed. The scope of this study is to solve path-following problems when AUVs are exposed to current disturbances. Briefly, the study consists of 4 steps. First, the states of the AUV were estimated by developing a state estimation algorithm, then the controller was designed, and then the guidance laws were designed. Finally, when all of these algorithms were integrated, various paths were defined and the performances of the guidance laws were compared. First, a state estimation algorithm was developed to perform this task, and with the help of this algorithm, all states of the AUV used by other algorithms were calculated simultaneously and it was aimed to simulate a real AUV operation. In this study, a ready-made nonlinear dynamic model of the Remus-100 vehicle was used, and sensor models were developed in addition to this model. The state estimation task was carried out with EKF and the estimation process was successfully achieved, there are many performance comparison outputs related to this situation in the relevant chapter. Afterward, a controller was developed in which these state estimation outputs were provided as input, that is, estimated quantities in the real world, rather than dynamic model outputs, were input. Normally, in most studies in the literature, the references of the controllers are fed directly from the dynamic model, but in the real world, the problem cannot be approached this way because AUVs do not have the opportunity to measure or observe every state. In order to simulate this reality, the reference inputs of the controller were provided with the outputs of the EKF. LQR was used as the controller. However, when developing LQR, the model we have had to be a linear model, but the model we had was a nonlinear model. In order to design the LQR controller, this model was linearized using numerical linearization and then the LQR controller was developed. This controller was tested under various conditions and it was concluded that it performed very well. If we briefly talk about the development of guidance laws, which is one of the last steps of the study, LOS guidance law and its variants, ILOS and ALOS guidance laws, were developed in this

study. These developed guidance laws were tested separately and it was concluded that their performance was satisfactory. If we briefly talk about the design of the test scenarios, which is the last step of the study, 4 different paths were designed. A total of 4 paths were designed, namely straight, circular, semi-rectangular, and sinusoidal paths, respectively. Finally, these paths were tested under various current disturbance conditions and it was concluded that some guidance laws are more advantageous in certain situations. Briefly speaking, ILOS guidance law shows superior performance in circular and sinusoidal paths, which shows that ILOS guidance gives better results in paths containing curvature. It has been observed that LOS guidance giving good results on straight and semi-rectangular paths, which shows that LOS guidance gives better results on flat paths compared to other methods. In this case, it can be concluded that since the defined paths are predetermined paths, if there are straight lines in the planned path, LOS guidance can be used during this process, and ILOS guidance can be used actively in the parts of the path that contain curvatures, that is, in places where there are turns and maneuvers. This ultimately enables maximum path-following performance to be achieved in all designed paths. Since one guidance law performs better than the other according to the path features, automatic guidance law switching can be performed in AUV tasks by establishing a simple switch-case logic and achieving minimum cross-track error. One of the most important results of this study can be explained as follows: Depending on the characteristics of the defined path, the guidance law may change during the mission because the currently used guidance laws calculate the yaw angle command as a result of instantaneous calculations, that is, they do not contain any retrospective terms. Therefore, transitions between these algorithms do not create any discontinuity. Finally, all of the algorithms developed within the scope of this study have been developed to be used in real underwater vehicles, so I believe that the algorithms to be developed for Remus-100 in the future can be used as a reference source.

REFERENCES

[1] **Cohan, S.** (2008). Trends in rov development. Marine Technology Society Journal, 42(1), 38-43. https://doi.org/10.4031/002533208786861335

[2] **Xiao, C., Zhong, L., Jianqiang, Z., Dechao, Z., & Jiao, D.** (2018). Adaptive sliding-mode path following control system of the underactuated USV under the influence of ocean currents. Journal of Systems Engineering and Electronics,29(6), 1271. https://doi.org/10.21629/JSEE.2018.06.14

[3] **Jiang, Y., Guo, C., & Yu, H.** (2018). Horizontal trajectory tracking control for an underactuated AUV adopted global integral sliding mode control. 2018 Chinese Control And Decision Conference (CCDC), 5786-5791. https://doi.org/10.1109/CCDC.2018.8408142

[4] **Belleter, D., Maghenem, M. A., Paliotta, C., & Pettersen, K. Y.** (2019). Observer based path following for underactuated marine vessels in the presence of ocean currents: A global approach. Automatica, 100, 123-134. https://doi.org/10.1016/j.automatica.2018.11.008

[5] **Moe, S., Caharija, W., Pettersen, K. Y., & Schjolberg, I.** (2014). Path following of underactuated marine surface vessels in the presence of unknown ocean currents. 2014 American Control Conference, 3856-3861. https://doi.org/10.1109/ACC.2014.6858984

[6] **Kim, M. J., Baek, W.-K., Ha, K. N., & Joo, M. G.** (2015). Way-point tracking for a hovering AUV by PID controller. 2015 15th International Conference on Control, Automation and Systems (ICCAS), 744-746. https://doi.org/10.1109/ICCAS.2015.7364719

[7] **Aguiar, A. P., & Pascoal, A. M.** (2007). Dynamic positioning and way-point tracking of underactuated AUVs in the presence of ocean currents. International Journal of Control, 80(7), 1092-1108. https://doi.org/10.1080/00207170701268882

[8] **Elmokadem, T., Zribi, M., & Youcef-Toumi, K.** (2019). Control for dynamic positioning and way-point tracking of underactuated autonomous underwater vehicles using sliding mode control. Journal of Intelligent &RoboticSystems,95(3-4),1113-1132. https://doi.org/10.1007/s10846-018-0830-8

[9] **Zhang, Q., Lin, J., Sha, Q., He, B., & Li, G.** (2020). Deep interactive reinforcement learning for path following of autonomous underwater vehicle. lIEEE Access, 8, 24258-24268. https://doi.org/10.1109/ACCESS.2020.2970433

[10] **Yu, R., Shi, Z., Huang, C., Li, T., & Ma, Q.** (2017). Deep reinforcement learning based optimal trajectory tracking control of autonomous underwater vehicle. 2017 36th Chinese Control Conference (CCC), 4958-4965. https://doi.org/10.23919/ChiCC.2017.8028138

[11] **Wang, L., Zhang, L., Jia, H., & Wang, H.** (2012). Horizontal Tracking Control for AUV Based on Nonlinear Sliding Mode. International Conference on Information and Automation, 460-463. https://doi.org/https://doi.org/10.1109/ICInfA.2012.6246850

[12] **Ashrafiuon, H., & Muske, K. (**2008). Sliding Mode Tracking Control of Surface Vessels. 2008 American Control Conferance, 556-561. https://doi.org/10.1109/ACC.2008.4586550

[13] **Joe, H., Kim, M., & Yu, S.** (2014). Second-order sliding-mode controller for autonomous underwater vehicle in the presence of unknown disturbances. Nonlinear Dynamics, 78(1), 183-196. https://doi.org/10.1007/s11071-014-1431-0

[14] **Lapierre, L., & Jouvencel, B.** (2008). Robust nonlinear path-following control of an auv. IEEE Journal of Oceanic Engineering, 33(2), 89-102. https://doi.org/10.1109/JOE.2008.923554

[15] **Gao, J., Liu, C., & Proctor, A.** (2016). Nonlinear model predictive dynamic positioning control of an underwater vehicle with an onboard USBL system. Journal of Marine Science and Technology, 21(1), 57-69. https://doi.org/10.1007/s00773-015-0332-3

[16] **Paliotta, C., Lefeber, E., Pettersen, K. Y., Pinto, J., Costa, M., & de Figueiredo Borges de Sousa, J. T.** (2019). Trajectory tracking and path following for underactuated marine vehicles. IEEE Transactions on Control Systems Technology, 27(4), 1423-1437. https://doi.org/10.1109/TCST.2018.2834518

[17] **Kim, E., Fan, S., & Bose, N.** (2018). Estimating water current velocities by using a model-based high-gain observer for an autonomous underwater vehicle. IEEE Access, 6, 70259-70271. https://doi.org/10.1109/ACCESS.2018.2879469

[18] **Allotta, B., Caiti, A., Costanzi, R., Fanelli, F., Fenucci, D., Meli, E., & Ridolfi, A.** (2016). A new AUV navigation system exploiting unscented Kalman filter. Ocean Engineering, 113, 121-132. https://doi.org/10.1016/j.oceaneng.2015.12.058

[19] **Kim, J.** (2020). Cooperative localization and unknown currents estimation using multiple autonomous underwater vehicles. IEEE Robotics and Automation Letters, 5(2), 2365-2371. https://doi.org/10.1109/LRA.2020.2972889

[20] **Teo, K., An, E., & Beaujean, P.-P. J.** (2012). A robust fuzzy autonomous underwater vehicle (Auv) docking approach for unknown current disturbances. IEEE Journal of Oceanic Engineering, 37(2), 143-155. https://doi.org/10.1109/JOE.2011.2180058

[21] **Osborn, J., Qualls, S., Canning, J., Anderson, M., Edwards, D., & Wolbrecht, E.** (2015). AUV state estimation and navigation to compensate for ocean currents. OCEANS 2015 - MTS/IEEE Washington, 1-5. https://doi.org/10.23919/OCEANS.2015.7401906

[22] **Allotta, B., Costanzi, R., Fanelli, F., Monni, N., Paolucci, L., & Ridolfi, A.** (2017). Sea currents estimation during AUV navigation using

Unscented Kalman Filter. IFAC-PapersOnLine, 50(1), 13668-13673. https://doi.org/10.1016/j.ifacol.2017.08.2528

[23] **Zhang, G., Yan, W., Gao, J., & Liu, C.** (2016). High-gain observer-based model predictive control for cross tracking of underactuated autonomous underwater vehicles. 2016 IEEE International Conference on Underwater System Technology: Theory and Applications (USYS), 115-120. https://doi.org/10.1109/USYS.2016.7893920

[24] **Shen, C., Shi, Y., & Buckham, B.** (2018). Trajectory tracking control of an autonomous underwater vehicle using lyapunov-based model predictive control. IEEE Transactions on Industrial Electronics, 65(7), 5796-5805. https://doi.org/10.1109/TIE.2017.2779442

[25] **Yang, Y. C., Yang, K. S., Chen, C. Y., Mu, L. J., Chiu, Y. M., Yu, C. M., & Yang, W. C.** (2013). Robust trajectory control for an autonomous underwater vehicle. 2013 MTS/IEEE OCEANS - Bergen, 1-9. https://doi.org/10.1109/OCEANS-Bergen.2013.6607946

[26] **Lakhekar, G. V., & Saundarmal, V. D.** (2013). Robust self tuning of fuzzy sliding mode control. 2013 Fourth International Conference on Computing, Communications and Networking Technologies (ICCCNT), 1-7. https://doi.org/10.1109/ICCCNT.2013.6726610

[27] **Capron, B. D. O., & Odloak, D.** (2018). A robust LQR-MPC control strategy with input constraints and control zones. Journal of Process Control, 64, 89-99. https://doi.org/10.1016/j.jprocont.2018.02.008

[28] **Herlambang, T., Rahmalia, D., Nurhadi, H., Adzkiya, D., & Subchan, S.** (2020). Optimization of linear quadratic regulator with tracking applied to autonomous underwater vehicle (Auv) using cuckoo search. Nonlinear Dynamics and Systems Theory, 20(3), 282-298. https://scholar.its.ac.id/en/publications/optimization-of-linear-quadratic-regulator-with-tracking-applied-

[29] **Al Makdah, A. A. R., Daher, N., Asmar, D., & Shammas, E.** (2019). Three-dimensional trajectory tracking of a hybrid autonomous underwater vehicle in the presence of underwater current. Ocean Engineering, 185, 115-132. https://doi.org/10.1016/j.oceaneng.2019.05.030

[30] **Al Makdah, A. A., Shammas, E., Daher, N., & ElHajj, I.** (2016). Modeling and optimal three-dimensional trajectory tracking for an autonomous underwater vehicle. 2016 IEEE International Conference on Advanced Intelligent Mechatronics (AIM), 172-177. https://doi.org/10.1109/AIM.2016.7576762

[31] **Wang, S., Jin, H., Meng, L., & Li, G.** (2016). Optimize motion energy of AUV based on LQR control strategy. 2016 35th Chinese Control Conference (CCC), 4615-4620. https://doi.org/10.1109/ChiCC.2016.7554068

[32] **Zeng, J., Wan, L., Li, Y., Dong, Z., & Zhang, Y.** (2017). Adaptive line-of-sight path following control for underactuated autonomous underwater vehicles in the presence of ocean currents. International Journal of Advanced Robotic Systems, 14(6), 172988141774812. https://doi.org/10.1177/1729881417748127

[33] **Fossen, T. I.** (2023). An adaptive line-of-sight (Alos) guidance law for path following of aircraft and marine craft. IEEE Transactions on Control Systems Technology, 31(6), 2887-2894. https://doi.org/10.1109/TCST.2023.3259819

[34] **Fossen, T. I., & Lekkas, A. M.** (2017). Direct and indirect adaptive integral line-of-sight path-following controllers for marine craft exposed to ocean currents. International Journal of Adaptive Control and Signal Processing, 31(4), 445-463. https://doi.org/10.1002/acs.2550

[35] **Caharija, W., Pettersen, K. Y., Gravdahl, J. T., & Børhaug, E.** (2012). Integral LOS guidance for horizontal path following of underactuated autonomous underwater vehicles in the presence of vertical ocean currents. 2012 American Control Conference (ACC), 5427-5434. https://doi.org/10.1109/ACC.2012.6315607

[36] **Børhaug, E., Pavlov, A., & Pettersen, K.** (2008). Integral LOS control for path following of underactuated marine surface vessels in the presence of constant ocean currents. IEEE Conference on Decision and Control. https://doi.org/ 10.1109/CDC.2008.4739352

[37] **REMUS 100. (**2024). Woods Hole Oceanographic Institution. Retrived from: https://www2.whoi.edu/site/osl/vehicles/remus-100/

[38] **Cybergalactic.** (n.d.). REMUS 100 model. GitHub. Retrieved May 17, 2024, fromhttps://github.com/cybergalactic/MSS/blob/master/VESSELS/models/remus100.m

[39] **Osborn, J.** (2016). Auv state estimation, navigation, and control in the presence of ocean currents [Text]. Theses and Dissertations Collection. https://www.lib.uidaho.edu/digital/etd/items/osborn_idaho_0089n_10942.html

[40] **Kirk, D. E.** (2004). Optimal control theory: An introduction. Dover Publications.

[41] **Stevens, B. L., Lewis, F. L., & Johnson, E. N.** (2016). Aircraft control and simulation.

[42] **Gu, N., Wang, D., Peng, Z., Wang, J., & Han, Q.-L.** (2023). Advances in line-of-sight guidance for path following of autonomous marine vehicles: An overview. IEEE Transactions on Systems, Man, and Cybernetics: Systems, 53(1), 12-28. https://doi.org/10.1109/TSMC.2022.3162862

CURRICULUM VITAE

Name Surname : Muhammet AKAN

EDUCATION :

- **B.Sc. :** 2021, ITU, Aeronautical and Astronautical Engineering Faculty, Aeronautical Engineering Department
- **M.Sc. :** 2024, ITU, Aeronautical and Astronautical Engineering Faculty, Aeronautical and Astronautical Engineering Department

PUBLICATIONS, PRESENTATIONS AND PATENTS ON THE THESIS:

- **Akan, M.** 2023. Estimation of AUV States and Sea Current Components by Extended Kalman Filter in the Presence of Unknown Disturbances. İTU International Graduate Research Symposium May 17-20, 2023 İstanbul, Turkey.